LITHOS 488–489 (2024) 107820

Contents lists available at ScienceDirect

LITHOS

journal homepage: www.elsevier.com/locate/lithos

Research Article

PGE-Ni-Cu sulphide segregation by interaction of basaltic melt and peridotite xenoliths of the Catalan Volcanic Zone (Spain)

Miguel Roquet [a,*], Erwin Schettino [b], Marc Campeny [c], José María González-Jiménez [a], Michel Grégoire [d], Rubén Piña [e], Mathieu Leisen [d], Joaquín A. Proenza [f], Oscar Laurent [d], Llorenç Planagumà [g], Xavier Llovet [h]

[a] Instituto Andaluz de Ciencias de la Tierra, Consejo Superior de Investigaciones Científicas-Universidad de Granada, Avenida de las Palmeras 4, 18100 Armilla, Andalucía, Spain
[b] Department of Earth Sciences, ETH Zürich, Clausiusstrasse 25, 8092 Zürich, Switzerland
[c] Departament de Mineralogia, Museu de Ciències Naturals de Barcelona, Passeig Picasso s/n, 08003 Barcelona, Catalonia, Spain
[d] Geosciences Environnement Toulouse, CNRS-CNES-IRD-UPS, Observatoire Midi Pyrénées, 14 Avenue Edouard Belin, 31200 Toulouse, France
[e] Departamento de Cristalografía y Mineralogía, Facultad de Ciencias Geológicas, Universidad Complutense de Madrid, c/ José Antonio Novais s/n, 28040, Madrid, Madrid, Spain
[f] Departament de Mineralogia, Petrologia i Geologia Aplicada, Universitat de Barcelona, Martí i Franquès s/n, 08028 Barcelona, Catalonia, Spain
[g] Tosca, Environment Services of Education, Casal dels Volcans, Av. Santa Coloma, 17800 Olot, Catalonia, Spain
[h] Centres Científics i Tecnològics, Universitat de Barcelona, Lluís Solé i Sabarís, 08028 Barcelona, Catalonia, Spain

ARTICLE INFO

Keywords:
Sulphides
Mantle xenoliths
Metasomatism
Subcontinental lithospheric mantle
Catalan Volcanic Zone

ABSTRACT

Spinel lherzolite xenoliths from the Sant Corneli volcano (Catalan Volcanic Zone, NE Spain) carry the geochemical imprint of melt/rock reaction events that have affected the subcontinental lithospheric mantle (SCLM) beneath the northeastern Iberian margin. Trace element signatures of clinopyroxene indicate that this volume of the SCLM initially experienced low degrees (F = 8 %) of partial melting, followed by extensive refertilization by alkaline silicate melts undergoing chromatographic fractionation while percolating through the mantle peridotites. Furthermore, the presence of interstitial sulphide-bearing silicate glass, as well as secondary coronitic rims around mantle minerals, records the melt/rock reaction product associated with the infiltration of the host alkaline basalts while erupting to the surface. Abundant irregular/blocky sulphides located within the interstitial glass patches are comprised of myrmekitic intergrowths of pentlandite ± bornite ± chalcopyrite, suggesting their derivation from immiscible droplets of Fe-Ni-Cu sulphide melt transported by the host alkaline basalts. The variable chondrite-normalized platinum-group element (PGE) systematics and chalcogenes (Se, Te, As, Bi and Sb) abundances of these sulphides track two distinct transport mechanisms for their parental sulphide melts: 1) by unmixing of Ni-Cu-rich sulphide liquid in alkaline basalts attaining sulphide-saturation while interacting with the peridotite xenoliths, and 2) by mechanical transport of immiscible droplets of Ni-Cu-rich sulphide liquid originally extracted by residual monosulphide solid solution undergoing incongruent melting in their mantle source. In addition, many sulphides have PGE abundances that cannot be explained solely by solid-melt chemical partition coefficients but that were likely influenced by the mechanical entrapment, or early-magmatic segregation, of pre-existing PGE-rich nanoparticles or nanomelts. The geochemical signal of these mineral nanoparticles may significantly influence sulphides PGE distribution, sometimes resulting in pronounced positive anomalies in Ir—Rh, Au, or Ru—Rh, along with negative anomalies in Pt.

1. Introduction

Understanding how sulphides behave during melt percolation and melt/rock reaction is key for predicting how the siderophile and chalcophile precious metals (Au, Ag, Pt, Pd, Rh, Ru, Ir, Os) distribute and/or concentrate through the Earth's continental lithosphere (Holwell et al., 2022; Tassara et al., 2017, 2020). The mobility and reactivity of sulphides in magmatic processes govern the extent by which metals and

* Corresponding author.
E-mail address: mroquetp@correo.ugr.es (M. Roquet).

https://doi.org/10.1016/j.lithos.2024.107820
Received 30 January 2024; Received in revised form 17 September 2024; Accepted 20 September 2024
Available online 28 September 2024

sulphur are extracted from the mantle during partial melting processes (e.g., Ballhaus et al., 2006; Mavrogenes and O'Neill, 1999; Rielli et al., 2022). These processes also have consequences on the metal fluxes through the continental lithosphere by upwarding magmas (e.g., Blanks et al., 2020; Schettino et al., 2023) and their final crystallization in the form of shallow crustal ores (e.g., Hepworth et al., 2020; Holwell et al., 2019). Therefore, deciphering the behaviour of sulphides during melt percolation represents a key issue, yet still controversial, for assessing the budget of precious metals that can be potentially transferred from mantle-derived magmas to form ore mineralisations in the crust.

Most inferences on sulphide behaviour during melt percolation are extrapolated by applying experimentally-determined phase diagrams (Ballhaus et al., 2006; Bockrath et al., 2004; Helmy et al., 2021) to the interpretation of Fe-Ni-Cu base-metal sulphides (BMS), which are routinely observed in (ultra)-mafic rocks from the upper mantle (Alard et al., 2000, 2011; Delpech et al., 2012; Lorand and Alard, 2001) and crustal magmatic suites (Barnes et al., 2017). However, disentangling the main textural, compositional (e.g., Ni/[Ni + Fe] or metal/S ratios), and geochemical tracers (e.g., platinum-group element: PGE systematics; chalcogenes: Se, Te, As, Bi and Sb) for sulphide genesis in natural samples is often challenging (e.g., Alard et al., 2011; Delpech et al., 2012; Tassara et al., 2018). This difficulty frequently leads to complex relationships when these tracers are analysed within the context of the petrologic evolution of the surrounding mantle and/or magmatic rocks (Aulbach et al., 2004; González-Jiménez et al., 2014; Griffin et al., 2002; Hughes et al., 2017; Lorand et al., 2004; Savelyev et al., 2018; Schettino et al., 2022). Much of the uncertainty arises as equilibrium textures and chemical compositions in natural systems are generally dictated by a great number of different factors and mechanisms, which can overprint to a variable extent or even erase the primary signatures associated with sulphide precipitation/dissolution events. Additional complexity is related to whether the precious metals are fully dissolved or not in the sulphide liquid and/or their solid products (Anenburg and Mavrogenes, 2020). Indeed, recent work is providing compelling evidence that the transport of precious metals may preferentially take place in form of insoluble nanomelts and/or nanoparticles (González-Jiménez et al., 2019, 2020; Schettino et al., 2022, 2023), thus possibly not following conventional models based on sulphide-silicate chemical partition coefficients (e.g., Brenan et al., 2016; Mann et al., 2012). However, the geochemical implications of nanomelt/nanoparticle transport to the precious metals inventory of sulphide liquids in silicate magmas are still under debate.

Sulphide-bearing glassy patches in mantle xenoliths provide a direct perspective into the very early stages of melt/rock interaction in the mantle (e.g., Rielli et al., 2022). As they are rapidly brought to the surface by the host lavas, the xenoliths "freeze" the metasomatic mineral assemblage associated with the melt/peridotite interaction event(s) that eventually precipitated the interstitial sulphide-bearing glass (e.g., González-Jiménez et al., 2014, 2019; Ionov et al., 1994; Neumann and Wulff-Pedersen, 1997; Schettino et al., 2022, 2024; Shaw et al., 2006). Therefore, the study of glassy patches in mantle xenoliths offers a natural analogue of experimental work precipitating sulphides in response to the melt percolation and melt/rock reaction processes (Rielli et al., 2022).

In this work, we combine a petrographic and in-situ geochemical characterization of sulphide grains entrained in glassy patches from the Sant Corneli volcano peridotite xenoliths (Catalan Volcanic Zone, NE Spain). The results are discussed in order to unravel the petrogenesis of sulphides with respect to melt percolation in the mantle, as well as to elucidate its ultimate implications to the transport and storage of precious metals through the continental lithosphere.

2. Geological setting

Since the late Eocene up to the Pleistocene, an extensional tectonic period led to the formation of the European Cenozoic Rift System (ECRIS) (Dèzes et al., 2004; Martí et al., 1992; Wilson and Downes, 1992). The ECRIS spans approximately 2000 km from the south-western part of Poland to the eastern part of the Iberian Peninsula (Fig. 1a), and is directly connected to the development of several well-known volcanic occurrences across Europe, such as the Eifel Volcanic Field in Germany or the Central Massif in France (Dèzes et al., 2004). On the north-eastern margin of the Iberian Peninsula, this extensional setting is also linked to the occurrence of the Catalan Volcanic Zone (CVZ), considered the most recent magmatic phase of Neogene-Quaternary volcanism in north-eastern Iberian Peninsula (Martí et al., 1992; Martí et al., 2011). The CVZ, located beneath the eastern region of the Pyrenees range and spanning approximately ~100 km along the Mediterranean coast (Fig. 1b), is divided into three distinct sectors: (1) Empordà, (2) La Selva, and (3) La Garrotxa (Martí et al., 2011). The volcanic activity in the CVZ started in the Empordà sector (14 to 6 Ma), then moved towards La Selva (5 to 2 Ma), and eventually arrived to La Garrotxa (ca. 350.000 to 8.400 years ago; Martí et al., 2001; Revelles et al., 2023). Mantle xenoliths, primarily consisting of spinel peridotites and pyroxenites hosted in basic volcanic rocks, have been commonly reported in various CVZ localities (Cebriá et al., 2000; Fernández-Roig et al., 2016; Fernández-Roig and Galán, 2015; Galán et al., 2008). Roca (2001) suggested that the lithosphere beneath this region is approximately 60–70 km thick. Additionally, previous petrological studies suggested the occurrence of metasomatic alkaline melts that extensively affected the CVZ mantle xenoliths (Bianchini et al., 2007; Galán et al., 2008; Galán and Oliveras, 2014). However, other authors have also reported polyphase sulphides (pyrrhotite+chalcopyrite and pentlandite+chalcopyrite) in the CVZ xenoliths, defining their various microstructural positions: enclosed in silicates, within reaction rims, and embedded in the interstitial glass (Cruz et al., 2014).

In the present study, we focused on the examination of sulphide-bearing peridotite mantle xenoliths extruded by the Sant Corneli volcano, situated in the southernmost part of the CVZ sector of La Selva (Fig. 1b). The Sant Corneli volcano is associated with a late-Neogene volcanic pulse, forming a typical strombolian cone 185 m in height with a related basanite lava flow exhibiting well-defined columnar jointing (Fig. 2a, b). The volcano is currently only partially preserved due to extensive mining activity that permits the exposure of peridotite mantle xenoliths up to 15 cm in size (Fig. 2c, d).

3. Analytical procedures

3.1. Petrography and sampling

A suite of seven peridotite xenoliths were collected from the quarry of the Sant Corneli volcano in the southernmost part of the CVZ (Fig. 1b). A preliminary examination was carried out in an effort to identify petrographic features, using optical microscopy. Qualitative identification of mineral phases and detailed textural analysis were also conducted by high-resolution scanning electron microscopy (HRSEM) on carbon-coated thin sections, by using an AURIGA (Carl Zeiss SMT) SEM equipped with energy dispersive X-ray spectroscopy (EDS), and secondary electron and backscattered electron detectors at the Centro de Instrumentación Científica of the University of Granada (CIC-UGR). Operating conditions were 20 kV accelerating voltage and a 5 μm spot-size beam. Subsequently, using Oxford Instruments® software, the obtained spectra were compared to internal standards of the equipment to estimate the chemical concentrations.

3.2. In-situ major and trace elements

Major elements compositions were analysed using a JEOL JXA-8230 electron microprobe (EMPA) operated in wavelength-dispersive mode at the Scientific and Technological Centres of the University of Barcelona (CCiTUB). Three different analytical routines employing 20 kV accelerating voltage was used: one for silicates and spinel, another one for the

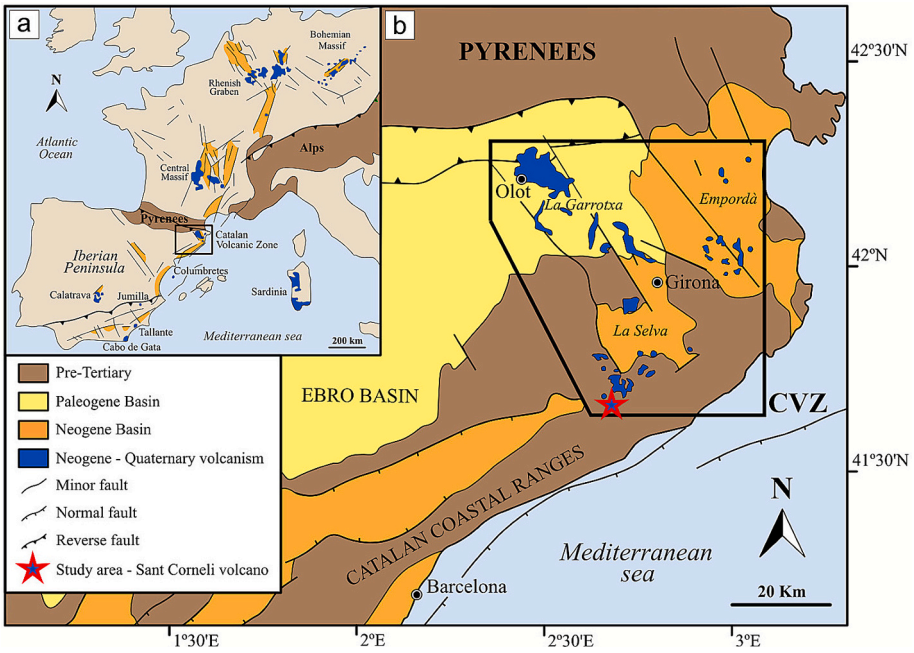

Fig. 1. a) Spatial distribution of tectonic structures associated with the European Cenozoic Rift in relation to primary outcrops of Neogene-Quaternary volcanic rocks. Map modified from Martí et al. (2001). b) Geological sketch map depicting the Catalan Volcanic Zone (CVZ; Martí et al., 2011) in northeastern Spain, indicating the locations of outcrops for various volcanic suites, including the area studied, where the Sant Corneli volcano is located. Map modified from Sedano (2019).

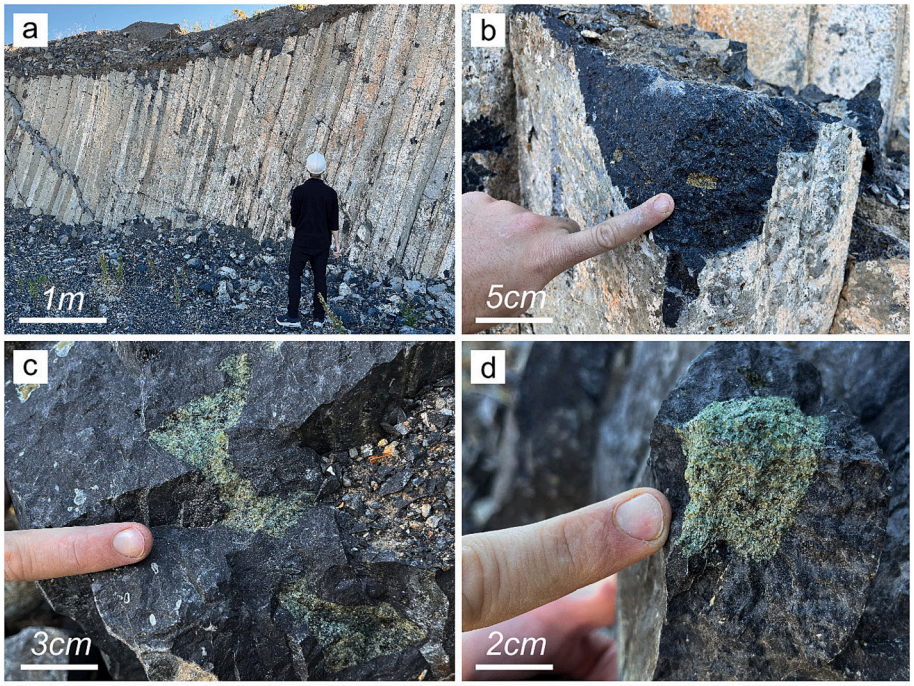

Fig. 2. a) General view of the Sant Corneli outcrop exhibiting basalt columnar jointing. b-d) Images of peridotitic mantle xenoliths enclosed in the basalts from the Sant Corneli volcano.

interstitial glass and a third one for sulphides. Silicates and spinel were analysed using a 15–20 nA beam current and a 5–10 μm spot size. Interstitial glass was analysed using a 6 nA beam current and a defocused 20 μm spot size. Sulphides were analysed using a 15 nA beam current and a defocused 5 μm spot. Counting times were 10 s peak and 10 s background for all analysed elements: S, As, Se, Fe, Co, Ni, Cu, Si, Al, Ca, K, Na, Mg, Mn, Zn, Ti, V, and Cr. The following crystals and X-ray lines were used: TAP (Si Kα, Al Kα), PETJ (Cr Kα, Ti Kα, S Kα), TAPH (Mg Kα, Na Kα, As Lα, Se Lα), PETL (K Kα, Ca Kα), LiFH (Fe Kα, Co Kα, Zn Kα, Cu Kα, V Kα), LiFL (Ni Kα, Cu Kα). Standards used for calibration were: diopside (Si), kyanite (Al), wollastonite (Ca), orthoclase (K), albite (Na), periclase (Mg), rhodonite (Mn), Fe_2O_x (Fe), NiO (Ni), ZnSe (Zn and Se), metallic V (V), Cr_2O_3 (Cr), FeS_2 (S, Fe), arsenopyrite (As), metallic Co (Co), metallic Ni (Ni), Cu_2S (Cu and S) and standard reference material SRM-1158 (Fe, Ni) (the SRM-1158 was used for phases with Ni contents greater than 20 wt%). Data reduction was performed using JEOL PC-

EMPA software with the XPP matrix correction and the FFAST mass attenuation coefficients. Results are presented in Supplementary Tables 1 and 2. X-ray maps of sulphide minerals were collected using 20 kV accelerating voltage, 20 nA beam current and 20–30 ms dwell time. X-ray maps were converted into concentration maps by applying the ZAF matrix correction.

Trace elements including rare earth elements (REE), Li, Ba, Rb, Cs, Sr, Th, U, Nb, Ta, Pb, Zr, Hf and Y) were determined in situ on clinopyroxene and interstitial glass in the polished thin sections, by laser-ablation inductively-coupled-plasma mass spectrometry (LA-ICP-MS). In particular, the analyses were carried out on the clinopyroxene cores and rims and on the interstitial glass in contact with them. These measurements were conducted at the laboratory of Géosciences Environnement Toulouse (GET), using an Element HR-ICPMS (ThermoScientific) coupled to a New Wave femtosecond laser (NWRfemto). The counting time for each analysis was 60 s (15 s for warmup and washout and 30 s of dwell time). The diameter of the laser beam spot was around 40 μm, the frequency 8 Hz and a fluence of 3 J/cm^2. Prior to each analysis session, the ICP-MS was tuned by ablating a NIST SRM 610 glass reference material (Jochum et al., 2011), to ensure acceptable levels of sensitivity, stability, oxide and fractionation (U/Th). Internal and external standards were performed at the beginning and at the end of each 15–20 spot analyses. Data reduction was performed using the Iolite 2.5 software package (Paton et al., 2011) on the IgorPro platform by careful inspection of time-resolved spectra to ensure homogeneity and stability of signals during the ablation time. Each analysis was normalized to Ca using concentrations determined by electron microprobe. Results are presented in Supplementary Table 3.

PGE and semi-metals (plus Au, Ag and Pb) were determined in sulphides (> 50 μm) by LA-ICP-MS. These analyses were performed at the LabMaTer of the Université du Quebec à Chicoutimi (UQAC), using an Excimer 193-nm Resolution M-50 with a double volume cell S-155 coupled with an Agilent 7900 mass spectrometer. The following isotopes were monitored ^{29}Si, ^{34}S, ^{51}V, ^{52}Cr, ^{55}Mn, ^{54}Fe, ^{57}Fe, ^{59}Co, ^{60}Ni, ^{65}Cu, ^{66}Zn, ^{73}Ge, ^{75}As, ^{82}Se, ^{95}Mo, ^{101}Ru, ^{103}Rh, ^{105}Pd, ^{107}Ag, ^{108}Pd, ^{111}Cd, ^{115}In, ^{118}Sn, ^{121}Sb, ^{125}Te, ^{128}Te, ^{189}Os, ^{193}Ir, ^{195}Pt ^{197}Au, ^{208}Pb, and ^{209}Bi. The analyses were conducted using an 11–25 μm beam diameter single spot, 15 Hz frequency, and a fluence of 3 J/cm^2. The ablated material was transported to the mass spectrometer by an argon-helium gas mix. Then, the material was analysed using the mass spectrometer in time resolution mode using mass jumping and a dwell time of 10 ms/peak. The duration of the analysis was 30 s for the gas blank and 60 s for the sulphide. Data reduction was carried out by using the Iolite package of Igor Pro 8.0 software (Paton et al., 2011). The isotope ^{57}Fe was used as internal standard. As irregular/blocky sulphides were commonly composed of different sulphides (e.g. pentlandite or chalcopyrite), we used the Fe content obtained by electron microprobe of the most abundant sulphide mineral. When two sulphides were equally proportional the laser totally ablated the whole composite grain and we used the reconstructed Fe content for the sulphide. For the calibration of PGE and Au, we used the certified reference material Laflamme Po-727 that consists of a synthetic FeS doped with 35–45 ppm of each element. For the calibration of the rest of elements, we used MASS-1 that consists of a Zn-Cu-Fe-S pressed powder pellet provided by the USGS and doped with 50–70 ppm of most chalcophile elements. The calibrations were monitored using GSE-1 g and UQAC-FeS1. GSE-1 g is a natural basaltic glass provided by the USGS doped with most elements at 300–500 ppm, and UQAC-FeS1 is an in-house Fe—S reference material doped with trace amounts of most chalcophile elements. Because Laflamme Po-727 and MASS-1 do not contain Ni, we used UQAC-FeS1 as reference material. Analysis of these materials agreed with the certified and working values shown in Supplementary Table 4. Polyatomic interferences of ^{61}Ni^{40}Ar on ^{101}Ru were corrected using UQAC-FeS1. Polyatomic interference of ^{63}Cu^{40}Ar on ^{103}Rh was corrected using ^{103}Rh measured in MASS-1, which contains 13.4 % ^{63}Cu but no ^{103}Rh. One percent Cu produced ~1.4 ppm Rh interference. To avoid ^{65}Cu^{40}Ar interference on ^{105}Pd, we used ^{108}Pd in Cu-rich analysis instead of ^{105}Pd. Interferences of ^{108}Cd on ^{108}Pd and ^{68}Zn^{40}Ar on ^{108}Pd were controlled by monitoring the laser spectra signal and they were neglected due to the low Cd and Zn abundances. Results are presented in Supplementary Table 4, and a couple of examples of time-resolved spectra are presented in Supplementary Figs. 1 and 2.

4. Results

4.1. Xenolith petrology and mineral chemistry

The studied xenoliths (n = 7) are spinel-lherzolites composed of olivine, orthopyroxene, clinopyroxene and spinel (Fig. 3; Supplementary Fig. 3; Supplementary Table 5). All rocks display a protogranular, fine-grained (<0.7 mm) texture characterized by curvilinear to interlobate grain boundaries (Fig. 3a-b). Abundant sulphide-bearing silicate glass forms interstitial pockets and veins around "primary" mantle minerals in all samples (Fig. 3c-d).

The major element compositions of rock-forming minerals in all samples cluster within restricted and homogeneous compositional ranges (Supplementary Table 1). Olivine (n = 132) has Mg# [100 x Mg/(Mg + Fe^{2+})] between 88.1 and 90.7, coupled with elevated amounts of NiO (0.21–0.45 wt%) whereas CaO values were below detection limits (< 0.02 wt%). Orthopyroxene (n = 38) has significant Al_2O_3 (3.72–4.48 wt%) and low CaO (0.66–0.87 wt%) and Cr_2O_3 (0.25–0.48 wt%) contents, coupled with Mg# values (89.7–91.1) that are congruent with those of olivine. Clinopyroxene (n = 40) also shares similar Mg# (88.8–92.4), coupled with high Al_2O_3 (4.88–5.71 wt%) and Na_2O (0.91–1.31 wt%) and low TiO_2 contents (0.27–0.57 wt%) (Fig. 4a). The mineralogical characterization of pyroxenes using the Wo-En-Fe (wollastonite-enstatite-ferrosilite) ternary diagram allows us to classify orthopyroxenes as enstatites and clinopyroxenes as diopsides (Supplementary Fig. 4). Spinel (n = 35) is alumina-rich and Cr-poor (Cr# [Cr/(Cr + Al)] = 0.12–0.17), and has low Mg# (71.2–79.2) and TiO_2 (< 0.75 wt%) (Fig. 4b).

The rare earth element (REE) and trace element distributions in clinopyroxene show smooth, yet systematic variations between the different samples (Fig. 5; Supplementary Table 3). REE analyses were conducted on four out of the seven samples (n = 4), and these analyses define four distinct groups of mantle xenoliths, with each group corresponding exclusively to one of these samples:

- *Group A* clinopyroxene shows light REE (LREE)-depleted chondrite-normalized distributions ($[La/Sm]_N$ = 0.04–0.17; $[La/Yb]_N$ = 0.05–0.16), characterized by either flat middle-to-heavy REE (MREE-HREE) segments at ~10 times the chondritic proportions or by "hump-shaped" patterns with decreasing concentrations from MREE to HREE down to ~5 times the chondritic proportions (Fig. 5a). The primitive upper mantle (PUM)-normalized trace element patterns are characterized by pronounced negative anomalies of Sr and Zr relative to adjacent REEs, coupled with positive spikes in Th, U and Ta (Fig. 5b).
- *Group B* clinopyroxene exhibits nearly flat MREE-HREE distributions at ~10 times the chondritic proportions, coupled with slight depletion from Eu to Pr and steep positive inflections in most incompatible LREEs (i.e., La and Ce, $[La/Sm]_N$ = 0.22–2.61, Fig. 5a). The PUM-normalized trace element patterns are characterized by positive anomalies in Sr and Th—U and negative anomalies in Zr and Nb (Fig. 5b).
- *Group C* clinopyroxene shows concave-up chondrite-normalized patterns with supra-chondritic LREE/MREE ratios ($[La/Sm]_N$ = 1.71–3.03) and flat MREE-HREE segments (Fig. 5a). The PUM-normalized trace element distribution is very similar to those of group B, except for lacking the positive Sr anomalies (Fig. 5b).
- *Group D* clinopyroxene exhibits strongly LREE-enriched chondrite-normalized patterns ($[La/Sm]_N$ = 6.26–7.98; $[La/Yb]_N$ =

11.15–17.15), which resembles those of the other groups along the MREE-HREE segment (Fig. 5a). The PUM-normalized trace element distributions are characterized by positive spikes in Th—U and negative troughs in Nb—Ta (Fig. 5b).

4.2. Petrology and geochemistry of interstitial "glassy" patches and clinopyroxene coronitic rims

Abundant interstitial silicate glass was identified in all samples, forming lobate patches and vesicular pockets (~100–200 μm) that are interconnected by thin (~5–20 μm) intergranular veinlets and/or cracks (Fig. 6a-b). The glassy patches and veins are filled with abundant Mg-rich clay minerals covering the compositional range of saponite, which formed by low-temperature alteration of the original interstitial mafic/ultramafic glass. Moreover, the glass pockets (n = 141) are composed of a microcrystalline (<10 μm) assemblage of plagioclase, alkali feldspar, and minor olivine (Supplementary Table 1), likely originated by quenching of the interstitial melt upon host lava eruption. This microcrystalline groundmass is usually associated with reaction zones with the mantle peridotite assemblages, characterized by the presence of spongy textures and coronitic rims of "secondary" spinel and clinopyroxene around "primary" mantle minerals (Fig. 6c-d). The coronitic rims of clinopyroxene (n = 12) show scattered compositional ranges (Supplementary Fig. 4), characterized by increasing MgO (17.50–19.59 wt.) and Cr_2O_3 (0.52–1.33 wt%) with lowering Al_2O_3 (0.72–3.00 wt%), CaO (20.68–22.65 wt%) and Na_2O (0.31–0.52 wt%) compared with primary clinopyroxene (Fig. 4a). Likewise, the coronitic rims of spinel exhibit higher TiO_2 (0.23–2.05 wt%) and Cr# (0.20–0.36) and slightly lower Mg# (65.9–75.1) compared with the primary spinel (Fig. 4b).

The clinopyroxene rims show chondrite-normalized REE patterns that mimic, at higher chondritic-proportions, those of the corresponding primary clinopyroxene grains (*Groups B—D)* of xenoliths (Fig. 7). In general, their REE patterns are characterized by supra-chondritic LREE/HREE ratios ($[La/Yb]_N$ = 0.5–16.1) and negative Eu anomalies (Eu/Eu* = 0.26–0.87) (Fig. 7a-d). On the other hand, the surrounding glass patches display chondrite-normalized REE patterns characterized by lower MREE-HREE concentrations at ~1 times the chondritic proportions, coupled with variable LREE enrichment ($[La/Yb]_N$ = 1.59–52.52) and positive Eu anomalies (Eu/Eu* = 1.82–6.64) (Fig. 7a-d). The REE patterns in the glass patches resemble those characteristics of plagioclase and silicate glass in hybrid peridotites affected by basaltic melt infiltration (Rampone et al., 2020).

4.3. Characterization of sulphides in silicate glasses

Abundant sulphide grains of variable size (20–100 μm) are entrained within the glassy patches of Sant Corneli peridotite xenoliths (Fig. 6). The sulphide grains exhibit globular/droplet or irregularly-shaped, vermicular morphologies, and are typically intergrown with the secondary rims of clinopyroxene and spinel (Fig. 6). These irregular/blocky sulphides mostly consist of polymineralic myrmekitic intergrowths of pentlandite, chalcopyrite and bornite (Fig. 8a-d), which yield a variable range of major element compositions (Fig. 9a-c; Supplementary Table 2). Pentlandite is S-deficient (met/S = 1.05–1.13) with Ni/(Ni + Fe) = 0.43–0.68 (Fig. 10a), bornite (met/S = 1.28–1.52) covers the Fe-rich (Fe = 7.63–15.0 wt%) portion of the bornite-digenite (Cu_5FeS_4-Cu_9S_5) solid solution, whereas chalcopyrite is nearly stoichiometric (Fig. 10b). In addition to this, backscattered electron images (BSE) of polished thin sections reveal the presence of nano-to-micrometre sized euhedral inclusions with high average atomic number (bright colours), which are characterized by strong Pt, Au or Pb peaks in the energy dispersive X-ray spectra (Fig. 11a-d).

Three distinct types of sulphide populations may be recognized based on their noble metals (PGE and Au) and chalcogenes (As, Se, Sb, Te and Bi) systematics. These three distinct sulphide populations coexist within the same xenolith samples and share common morphological characteristics and textural location within the interstitial silicate glass. Therefore, they can only be distinguished based on their geochemical features. *Type 1* sulphides contains relatively high PGE abundances (∑PGE = 28.63–292.72 ppm; Fig. 12a-c) coupled with nearly-chondritic inter-element fractionation (Pd_N/Ir_N = 0.43–6.95; Fig. 12b), which yield flat chondrite-normalized PGE patterns characterized by variable Pt negative anomalies (Pt_N/Rh_N = 0.01–1.24;

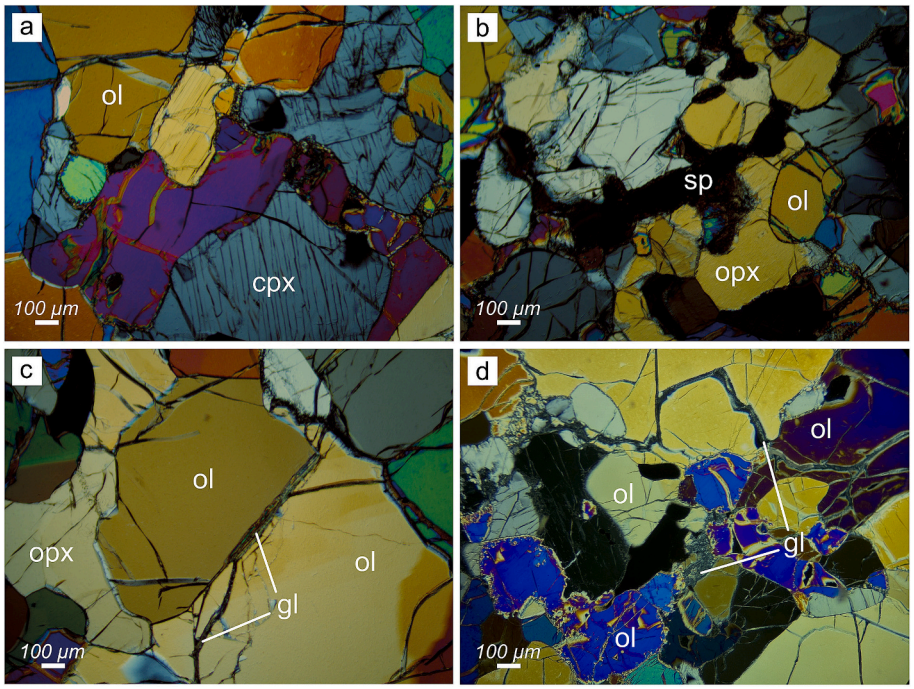

Fig. 3. Photomicrographs of polarized light optical microscope of Sant Corneli peridotite xenoliths. Mineral abbreviations: ol - olivine; sp. - spinel; cpx - clinopyroxene; opx - orthopyroxene; gl - glass. Sample codes: (a) SC01, (b) SC03, (c) SC04, (d) SC07.

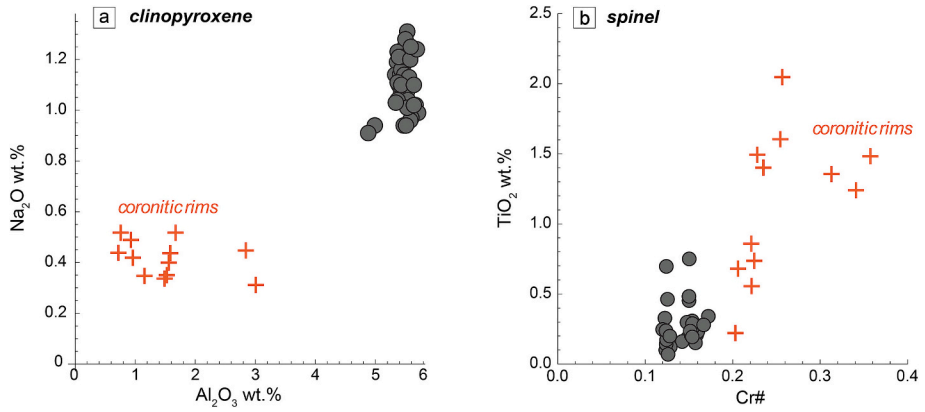

Fig. 4. Al_2O_3 (wt%) versus Na_2O (wt%) abundances in clinopyroxene grains (a) and Cr#[Cr/(Cr + Al)] versus TiO_2 (wt%) in spinel grains (b) of Sant Corneli peridotite xenoliths. Grey circles and orange crosses indicate the composition of cores and coronitic rims, respectively.

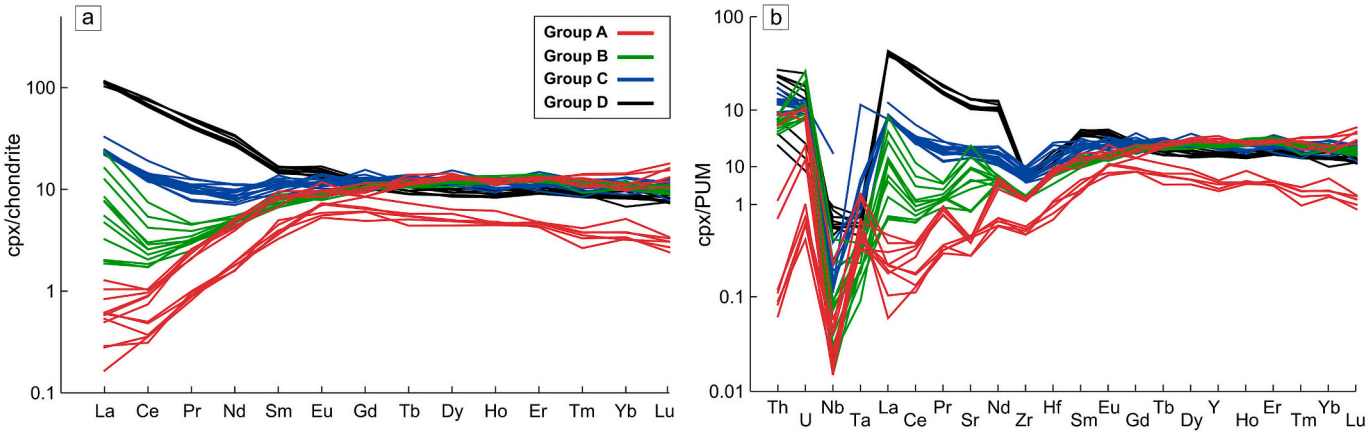

Fig. 5. Chondrite-normalized concentrations of rare earth elements (a) and primitive upper mantle-normalized trace element patterns (b) in clinopyroxene grains of spinel lherzolites from Sant Corneli, northeast Spain. Normalizing values from McDonough and Sun (1995).

Fig. 13a). *Type 2* sulphides exhibit lower PGE abundances compared to *type 1* (∑PGE = 0.91–32.55 ppm; Fig. 12a-c), which are negatively correlated to their bulk Cu/Ni ratios (Fig. 12a). These lower ∑PGE are especially due to decreasing IPGE contents (Ir-group: Os + Ir + Ru), which produce positively-sloped PGE patterns characterized by supra-chondritic Pd/Ir ratios (Pd_N/Ir_N = 9.85–38.69) and no Pt negative anomaly (Pt_N/Rh_N = 1.25–7.17; Fig. 13b). *Type 3* sulphides share geochemical characteristics in common with both *types 1* and *2* (Fig. 12). However, their chondrite-normalized PGE patterns differ from those of *types 1* and *2*, and in some cases, they present patterns with pronounced positive peaks in Ir—Rh, Ru—Rh, and Au (Fig. 13c-d).

All the three sulphide types share similar S/Se ratios (1315–9609; Fig. 12c), which encompass with the range previously reported for the primitive upper mantle (3300, McDonough and Sun, 1995) and other glass-entrained sulphides in mantle xenoliths (e.g., Alard et al., 2011; Delpech et al., 2012; Hughes et al., 2017). The extent of S/Se fractionation in Sant Corneli shows a rough positive correlation with the Cu/Ni ratios of *type 1* sulphides (Fig. 12d). A general trend of S/Se increase with decreasing Pd_N/Ir_N ratios is also observed for *type 3* sulphides (Fig. 12e), while all the three sulphide populations display tight negative correlation between S/Se and their concentrations of chalcogenes (TABS: Te, As, Bi, Sb and Se; Fig. 12f). A general trend of ∑PGE enrichment with increasing TABS contents, and viceversa, is observed for *type 1* and *type 2* sulphides, respectively (Fig. 12h). The total chalcogenes abundances are also positively correlated with the bulk Cu/Ni ratios of *type 2* sulphides (Fig. 12g), and with the extent of Pd_N/Ir_N fractionation of *type 3* sulphides (Fig. 12i).

5. Discussion

5.1. Nature of the subcontinental lithospheric mantle beneath the north-eastern Iberian margin

Clinopyroxene in Sant Corneli peridotite xenoliths show a wide range of trace element distributions, which record the partial melting and metasomatic history of the SCLM beneath NE Spain. The LREE-depleted patterns of clinopyroxene from *group A* xenoliths, coupled with their strong depletion in Nb, Zr and Sr (Fig. 5), are characteristics expected for solid residues affected by the progressive extraction of silicate melt (Norman, 1998). To constrain the conditions of partial melting for these peridotites, we compared the REE distributions of clinopyroxene in *group A* xenoliths with those modelled in a residual clinopyroxene according to fractional melting equations in a primitive upper mantle source (PUM, McDonough and Sun, 1995; Johnson et al., 1990). Low degrees (F = 8 %) of non-modal fractional melting in the spinel peridotite field effectively reproduce the LREE-depleted patterns of most clinopyroxene grains in *group A* xenoliths (Fig. 14a; Johnson et al., 1990). Such calculated melting degrees are consistent with the partial melting conditions previously inferred for other spinel-lherzolite xenoliths of the Catalan Volcanic Zone in NE Spain (Bianchini et al., 2007;Galán et al., 2008; Galán and Oliveras, 2014). Small deviations from the predicted melting curves are associated with the positive inflections in La (Fig. 14a), which are likely due to limited interaction between the residual clinopyroxene grains and LREE-enriched melt (Navon and Stolper, 1987). However, melting models in the spinel

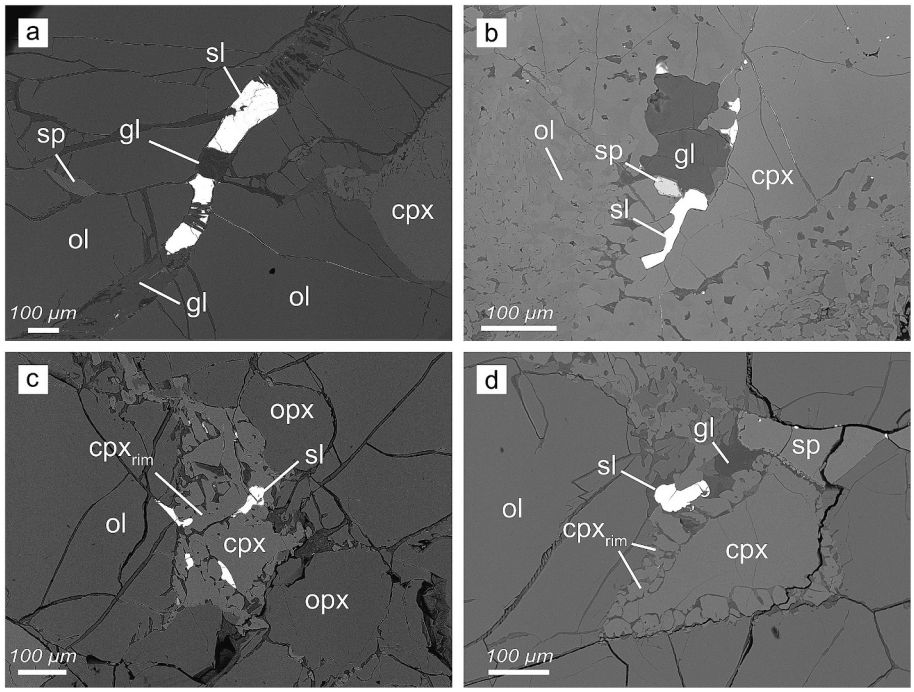

Fig. 6. Backscattered electron images showing the general microstructural characteristics of sulphide-bearing interstitial glassy patches in Sant Corneli peridotite xenoliths. a-b) Sulphide grains entrained within interstitial glass forming veins or cracks between silicate grains. c-d) Sulphide grains entrained within interstitial glass, in contact with silicates, forming spongy coronae textures. Mineral abbreviations: ol - olivine; cpx - clinopyroxene; opx - orthopyroxene; gl - glass; sl – sulphides; sp. – spinel. Sample codes: (a) SC04B, (b-d) SC01A.

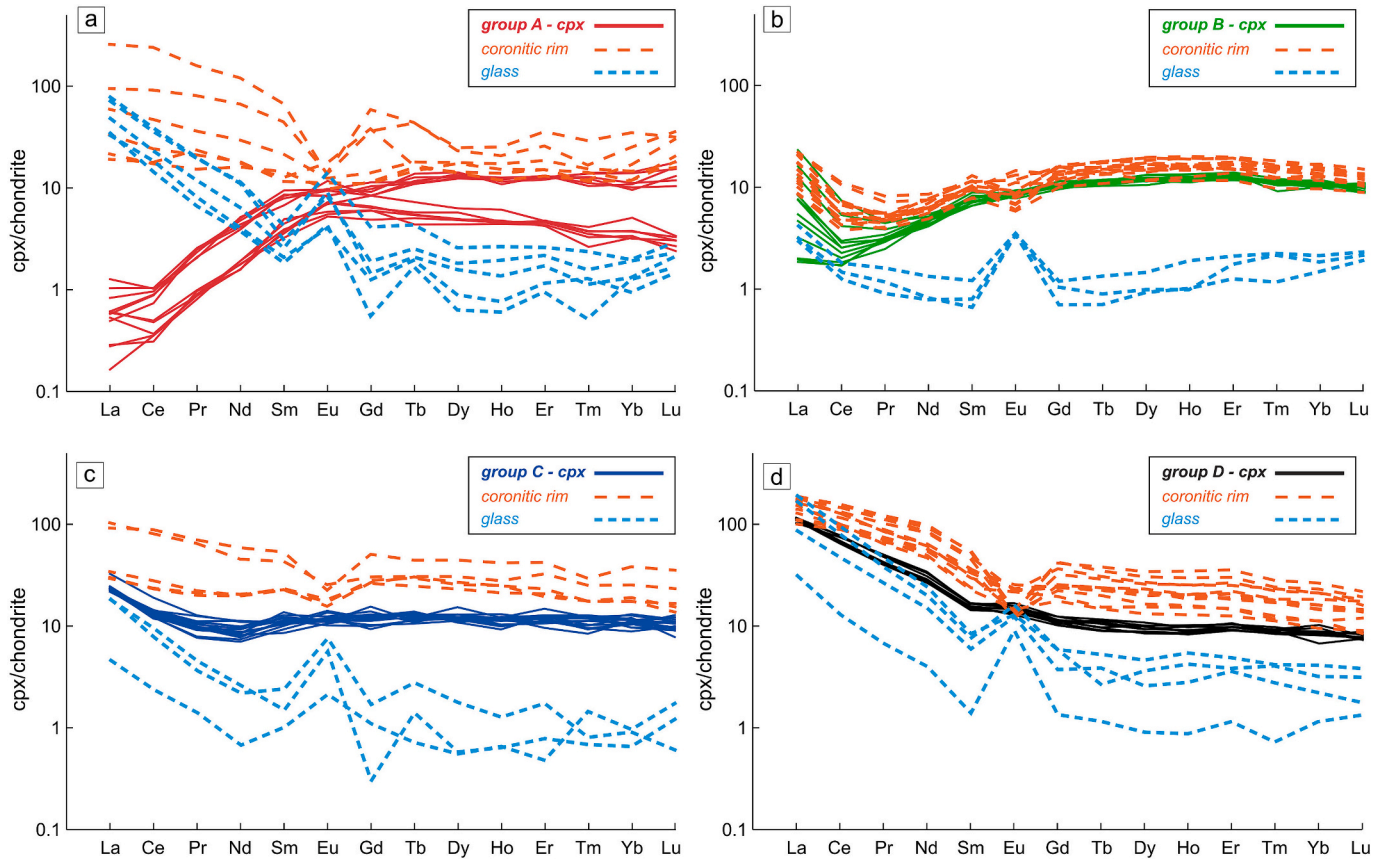

Fig. 7. Chondrite-normalized REE patterns for each clinopyroxene group compared with their surrounding coronitic rims and interstitial glassy patches. Normalizing values from McDonough and Sun (1995).

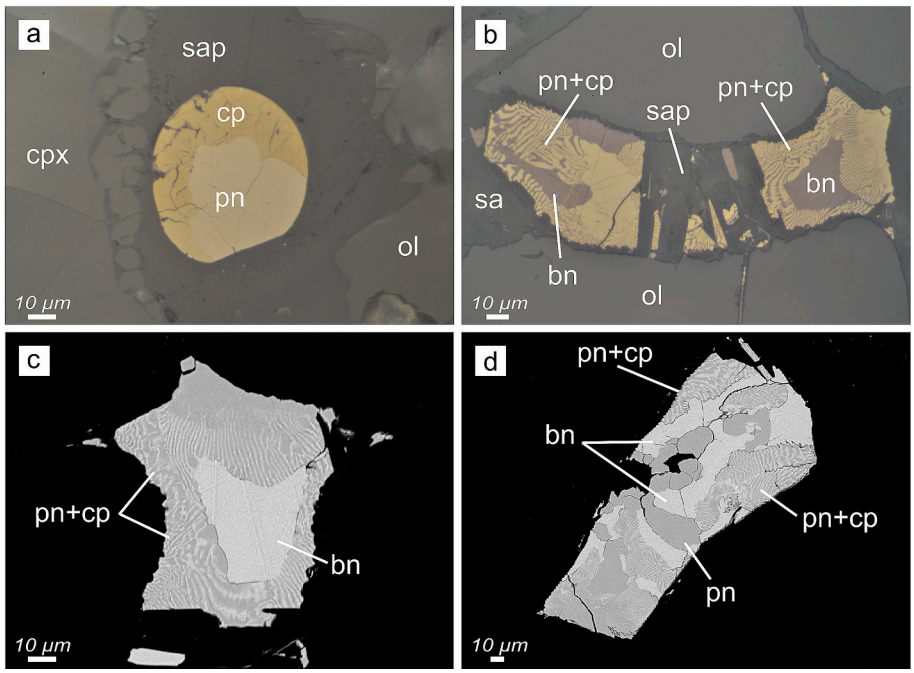

Fig. 8. Photomicrographs of reflect light optical microscope (a-b) and backscattered electron images (c-d) of sulphides entrained within interstitial glass veinlets. a) Sulphide droplet composed of chalcopyrite and pentlandite. b-d) Irregular sulphide grains composed of pentlandite, chalcopyrite, and bornite, exhibiting myrmekitic intergrowths. Mineral abbreviations: ol - olivine; cpx - clinopyroxene; sa - sanidine; sap - saponite; bn - bornite; pn - pentlandite; cp - chalcopyrite. Sample codes: (a) SC07B, (b-d) SC04B.

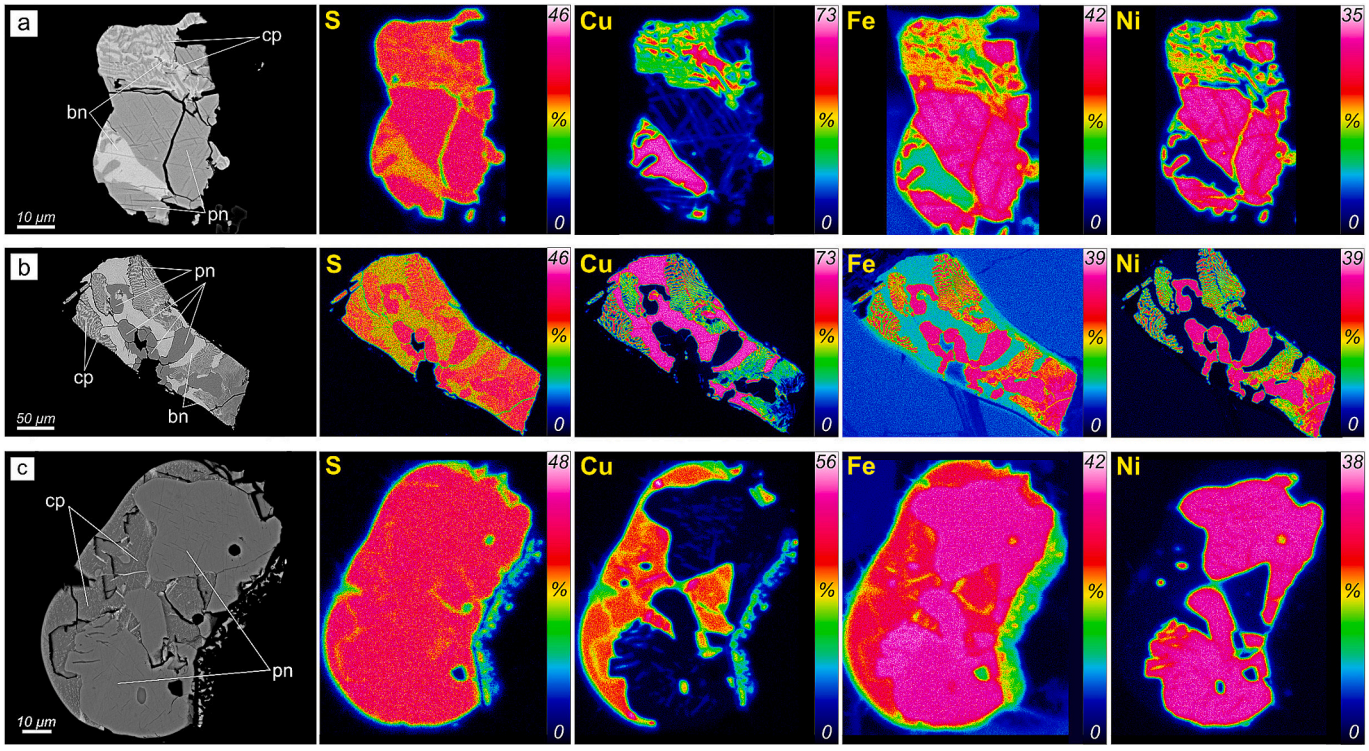

Fig. 9. Backscattered electron images depicting sulphides and their corresponding quantitative maps (in wt%) illustrating the distribution of major elements (S, Cu, Fe, Ni). Keys: cp: chalcopyrite; bn: bornite; pn: pentlandite.

peridotite field alone cannot account for those LREE-depleted clinopyroxene grains having "hump-shaped" REE patterns and supra-chondritic MREE/HREE ratios (Fig. 14a). Similar supra-chondritic MREE/HREE ratios in residual clinopyroxenes from spinel-lherzolite xenoliths of NE Spain, comparable to those observed in clinopyroxene from abyssal peridotites (Johnson et al., 1990), have been ascribed to melt extraction in the garnet peridotite stability field (Bianchini et al., 2007; Galán et al., 2008; Galán and Oliveras, 2014), due to the high compatibility of HREE for co-existing garnet (Hart and Dunn, 1993). Nevertheless, as soon as garnet breaks down during peridotite re-

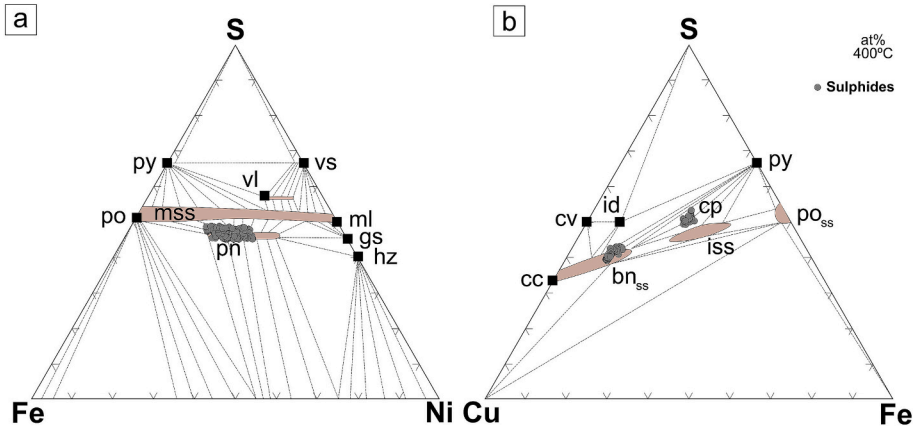

Fig. 10. Major element compositions of base metal sulphides (BMS) in Sant Corneli peridotite xenoliths plotted in the Fe-Ni-S (a) and Cu-Fe-S (b) phase diagrams. Phase relations at 400 °C are from Craig and Kullerud (1969) for the Fe-Ni-S system and Cabri (1973) for the Cu-Fe-S system. Mineral abbreviations: py - pyrite; po - pyrrhotite; po_{ss} - pyrrhotite solid solution; mss - monosulphide solid solution; pn - pentlandite; vl - violarite; vs - vaesite; ml - millerite; gs - godlevskite; hz - hazelwoodite; cc - chalcocite; cv - covellite; bn_{ss} - bornite solid solution; id - idaite; cp - chalcopyrite; iss - intermediate solid solution.

equilibration in the spinel stability field, the redistribution of HREEs between the spinel-facies mineral assemblages would hinder the preservation of the original "hump-shaped" REE patterns, yielding nearly flat MREE-HREE segments in the residual clinopyroxene (Hellebrand et al., 2002). According to Hellebrand et al. (2002), these types of REE patterns may arise in clinopyroxene as the mantle peridotites interact with very small volumes of depleted melt, due to the largest contribution of modal orthopyroxene to the whole-rock budget of HREEs.

Pervasive geochemical refertilization of the SCLM by interaction with percolating silicate melts is then witnessed by progressively increasing concentrations of most incompatible trace elements (LREE, Th, U) detected in clinopyroxene from *groups B*, *C* and *D* xenoliths (Fig. 5). In particular, these trace element patterns define a smooth spectrum of variations characterized by increasing LREE/HREE ratios with increasing Th—U abundances (Fig. 14b), producing a wide geochemical zoning typical of melt-infiltrated peridotites (Ionov et al., 2002; Borghini et al., 2023). This spectrum of geochemical distributions generally arises during a single event of melt percolation evolving at decreasing melt fractions (Schettino et al., 2022), which triggers the progressive chromatographic fractionation of most incompatible elements as the silicate melts migrate away from the main transport channel by reactive porous flow (Navon and Stolper, 1987; Oliveira et al., 2020). Indeed, the chromatographic fractionation model predicts that moderately compatible trace elements (e.g., HREE) are selectively removed by the silicate melt as it interacts with mantle minerals (Navon and Stolper, 1987), thus yielding a spectrum of metasomatic zoning dependent on the distance from the melt source (Bodinier et al., 1990). In this scenario, the composition of a percolating silicate melt progressively shifts towards enrichment in most incompatible elements (higher LREE/HREE, Th-U; Fig. 14b; Ionov et al., 2002), approaching the chemical equilibration with the peridotite minerals.

Previous inferences on the hypothetical metasomatic agents responsible for the geochemical refertilization of the SCLM in NE Spain were based on the equilibrium melt compositions computed from clinopyroxene/melt partitioning coefficients (Bianchini et al., 2007). These hypotheses encompassed Permo-Triassic alkaline magmas, tholeiitic dolerites associated with continental rifting events (Bianchini et al., 2007) and Cretaceous alkaline silicate melts evolving towards carbonatitic-rich melts (Galán et al., 2008; Galán and Oliveras, 2014). Our observations underpin the hypothesis that the SCLM beneath NE Spain was extensively re-fertilized during an alkaline metasomatic event, which involved the progressive differentiation of alkaline silicate melts becoming increasingly enriched in most incompatible elements as they migrate away from their magma source (Galán and Oliveras, 2014).

5.2. *Origin of sulphide-bearing silicate glass in mantle peridotites*

Sant Corneli peridotite xenoliths contain abundant glassy-like veins and patches filled with a micro-crystalline matrix of plagioclase, alkali feldspar, minor olivine and sulphides (Fig. 6a-d; Galán et al., 2008). The LREE-rich patterns, coupled with low MREE-HREE abundances and strong positive Eu anomalies of these micro-crystalline patches (Fig. 7a-d) are consistent with those characteristics of plagioclase-rich, silicate glass in mantle peridotites (Rampone et al., 2020), supporting the hypothesis that they precipitated from an interstitial silicate melt shortly before their rapid eruption. Whenever in contact with the "primary" mantle clinopyroxene and spinel, the silicate glass develops coronitic rims of "secondary" clinopyroxene and spinel (Fig. 6a-d), which are characterized by more refractory major element compositions (MgO-Cr_2O_3-rich and Al_2O_3-Na_2O-poor clinopyroxene, Cr#-rich spinel; Fig. 4a-b) and higher REE abundances (Fig. 7a-d). The distinct major and trace element compositions of these "spongy" coronae compared with those of the "primary" mineral assemblage (Fig. 4a-b, Fig. 7a-d) indicate that they formed through the chemical interaction between the interstitial silicate melt and the mantle peridotite (Pan et al., 2018), which likely occurred shortly before the eruption of the host alkaline basalts (Ionov et al., 1994).

Low degrees of in-situ melting of metasomatic assemblages often explain the SiO_2- and Al_2O_3-rich compositions of silicate glasses in mantle xenoliths (Ionov et al., 1994), as well as the generally "refractory" chemical characteristics of the co-existing clinopyroxene (higher MgO-Cr_2O_3, lower Al_2O_3-Na_2O) and spinel (higher Cr#) spongy coronae (Pan et al., 2018; Rielli et al., 2022; Schettino et al., 2022). However, this model cannot account for the genesis of the silicate glass in Sant Corneli xenoliths and the co-existing clinopyroxene spongy coronae, as the latter would have developed LREE-depleted patterns if formed by low degrees of partial melting (e.g., Schettino et al., 2022). Whereas, the REE over-abundances in the clinopyroxene rims, coupled with their increasing LREE/HREE ratios (Fig. 7a-d), suggest that they crystallized due to melt/rock reaction involving the metasomatic interaction between an infiltrating basaltic melt and the mantle peridotite (Miller et al., 2012; Neumann and Wulff-Pedersen, 1997; Shaw et al., 2006). The co-occurrence of pronounced positive Eu anomalies in the silicate glass and negative Eu anomalies in the coronitic rims of clinopyroxene hint to the chemical exchange during melt/rock reaction (Fig. 7a-d), which could have caused the preferential incorporation of Al_2O_3 and Na_2O in the plagioclase-rich matrix and corresponding depletion of these elements in the "refractory" coronitic rims of clinopyroxene (Fig. 4a). This mechanism properly accounts even for the Cr#- and TiO_2-rich compositions of the coronitic spinel rims (Fig. 4b),

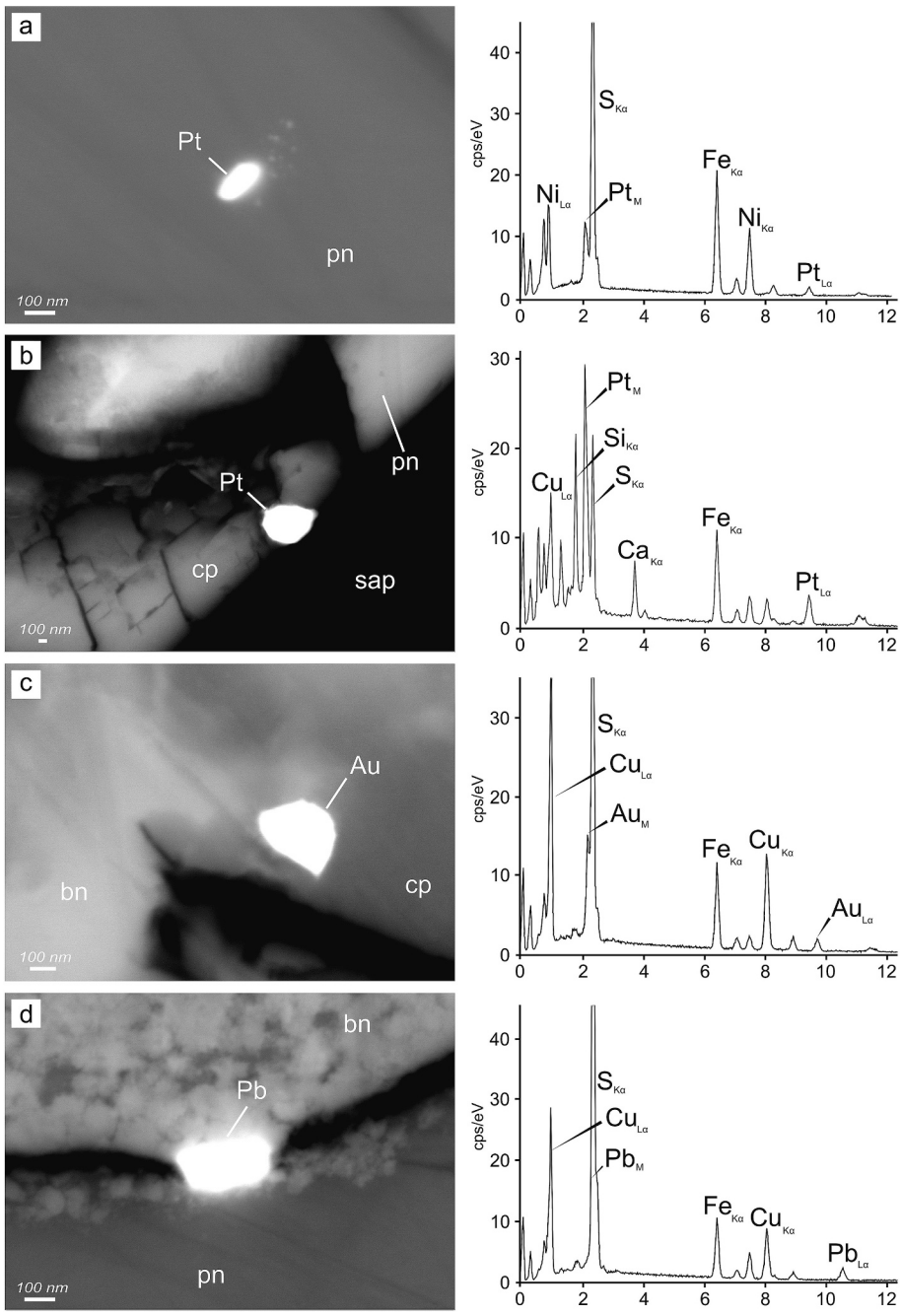

Fig. 11. Backscattered electron images and corresponding energy-dispersive X-ray spectroscopy spectra of sulphide hosted nanoparticles of platinum (a-b), native gold (c) and lead (d) in Sant Corneli peridotite xenoliths. Mineral abbreviations: pn - pentlandite; cp - chalcopyrite; bn - bornite; sap – saponite; cps - counts per second. Sample codes: (a) SC02B-4, (b) SC07B-10, (c) SC03A-10, (d) SC04B-6. (For interpretation of the references to colour in this figure legend, the reader is referred to the web version of this article.)

consistent with those generally documented for mantle spinel in plagioclase-impregnated peridotites (Rampone et al., 2020).

The widespread occurrence of these silicate glass patches through an inter-connected network of grain-boundary layers and veinlets suggest that this late-stage melt/rock reaction event occurred because of infiltration of the host alkaline-basalts (Neumann and Wulff-Pedersen, 1997; Schettino et al., 2024). Indeed, mass balance calculations between melt-precipitated mineral phases and their hypothetical modal proportions (e.g., 60 % clinopyroxene +40 % plagioclase) yield reconstructed REE distributions of the original interstitial melt that approach those of the Quaternary alkaline basalts of La Garrotxa volcanic field (Fig. 15; Cebriá et al., 2000). Thus, all these observations support the idea that sulphide-bearing silicate glass in Sant Corneli xenoliths formed by late-stage melt/rock reaction event associated with the infiltration of the host alkaline basalts in the peridotite xenoliths shortly before their fast eruption to the surface (González-Jiménez et al., 2014; Shaw et al., 2006; Tassara et al., 2018). The crystallization conditions of the clinopyroxene coronitic rims were determined by employing the clinopyroxene-only thermometer of Nimis and Taylor (2000) and cpx-barometer of Putirka (2008). The calculated values range between 3.9 and 10.6 kbar and 1110–1282 °C and likely reflect the P-T conditions of the late-stage melt/rock reaction event associated with the precipitation of the sulphide-bearing silicate glass patches (Bertotto et al., 2022). The inferred P-T conditions of the sulphide-bearing silicate

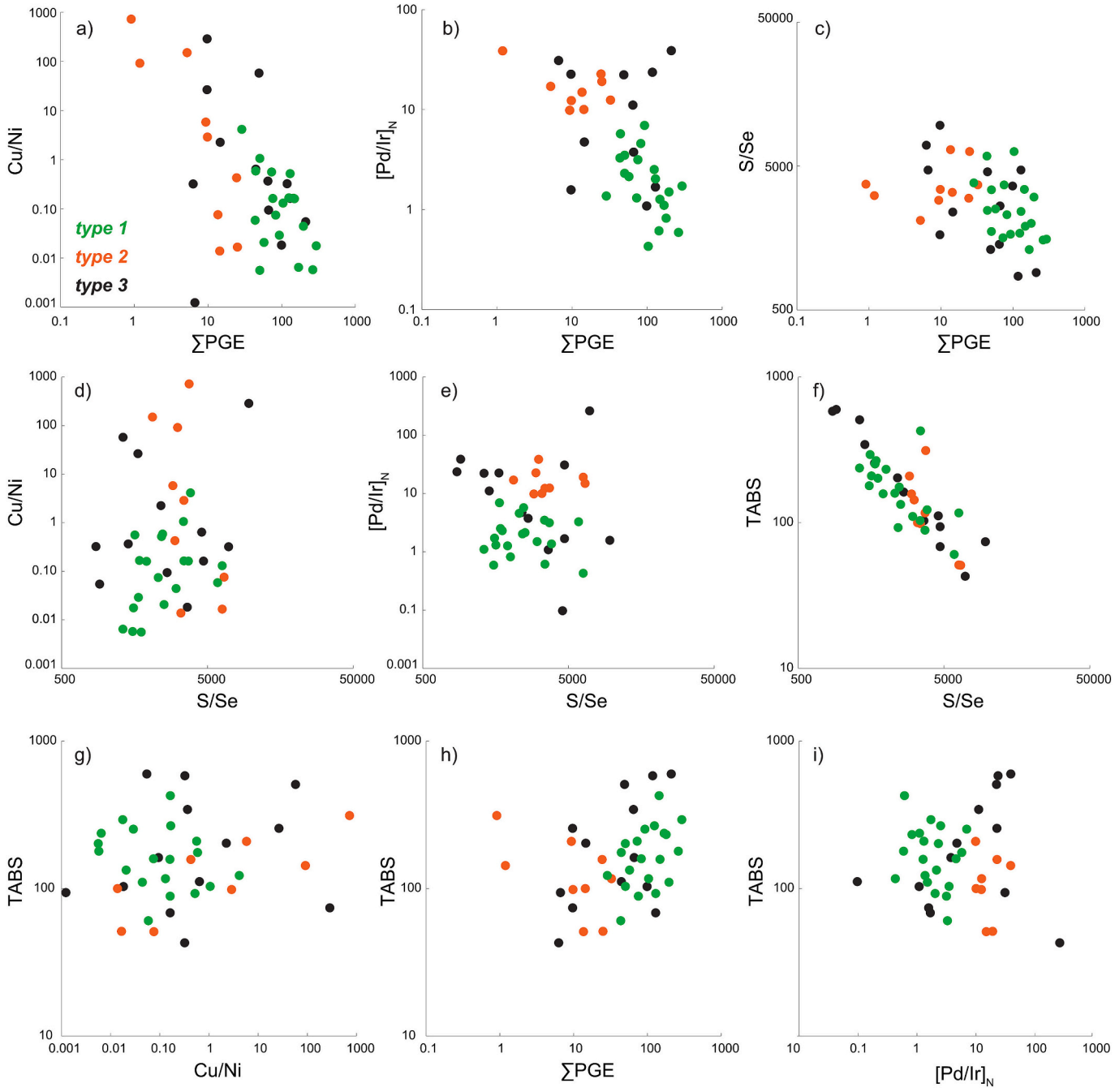

Fig. 12. In-situ trace element data of glass-entrained sulphides (*type 1* – green dots; *type 2* – orange dots; *type 3* – black dots) in Sant Corneli mantle xenoliths. Total PGE and Au abundances (∑PGE) vs. Cu/Ni ratios (a), chondrite-normalized Pd_N/Ir_N ratios (b), and S/Se (c). S/Se ratios vs. Cu/Ni (d), chondrite-normalized Pd_N/Ir_N ratios (e) and chalcogenes abundances (TABS: Te, As, Sb, Bi and Se) (f). Co-variation of TABS abundances vs. Cu/Ni (g), ∑PGE (h) and chondrite-normalized Pd_N/Ir_N ratios (i). (For interpretation of the references to colour in this figure legend, the reader is referred to the web version of this article.)

glasses are thus consistent with their formation by host-basalt infilitration upon xenolith ascent at surface.

5.3. *Mechanisms of sulphide transport during melt percolation in the mantle*

Sulphides in Sant Corneli xenoliths are systematically associated with the interstitial silicate glass and the coronitic rims of clinopyroxene and spinel, which ultimately formed as the host alkaline basalts infiltrated the peridotite xenoliths upon their fast eruption to the surface. These microstructural characteristics, coupled with their irregular shapes or droplet-like morphologies, suggest that these sulphides precipitated from immiscible droplets of a parental sulphide liquid, which was transported by the host alkaline basalts while infiltrating the peridotite xenoliths (Delpech et al., 2012; Hughes et al., 2017; Schettino et al., 2024; Tassara et al., 2018). The pentlandite ± bornite ± chalcopyrite paragenesis reported in Sant Corneli xenoliths (Figs. 8–10), together with general lack of pyrrhotite, cannot be addressed by the subsolidus re-equilibration of a former monosulphide solid solution (*mss*), which is the only sulphide mineral that can potentially solidify under the P-T conditions in which the xenoliths equilibrated (Fig. 16; Craig and Kullerud, 1968; Helmy et al., 2021). Rather, the Ni-Cu-rich compositions of the sulphides point to their derivation from a parental liquid composition overlapping with the central portion of the Fe-Ni-Cu-

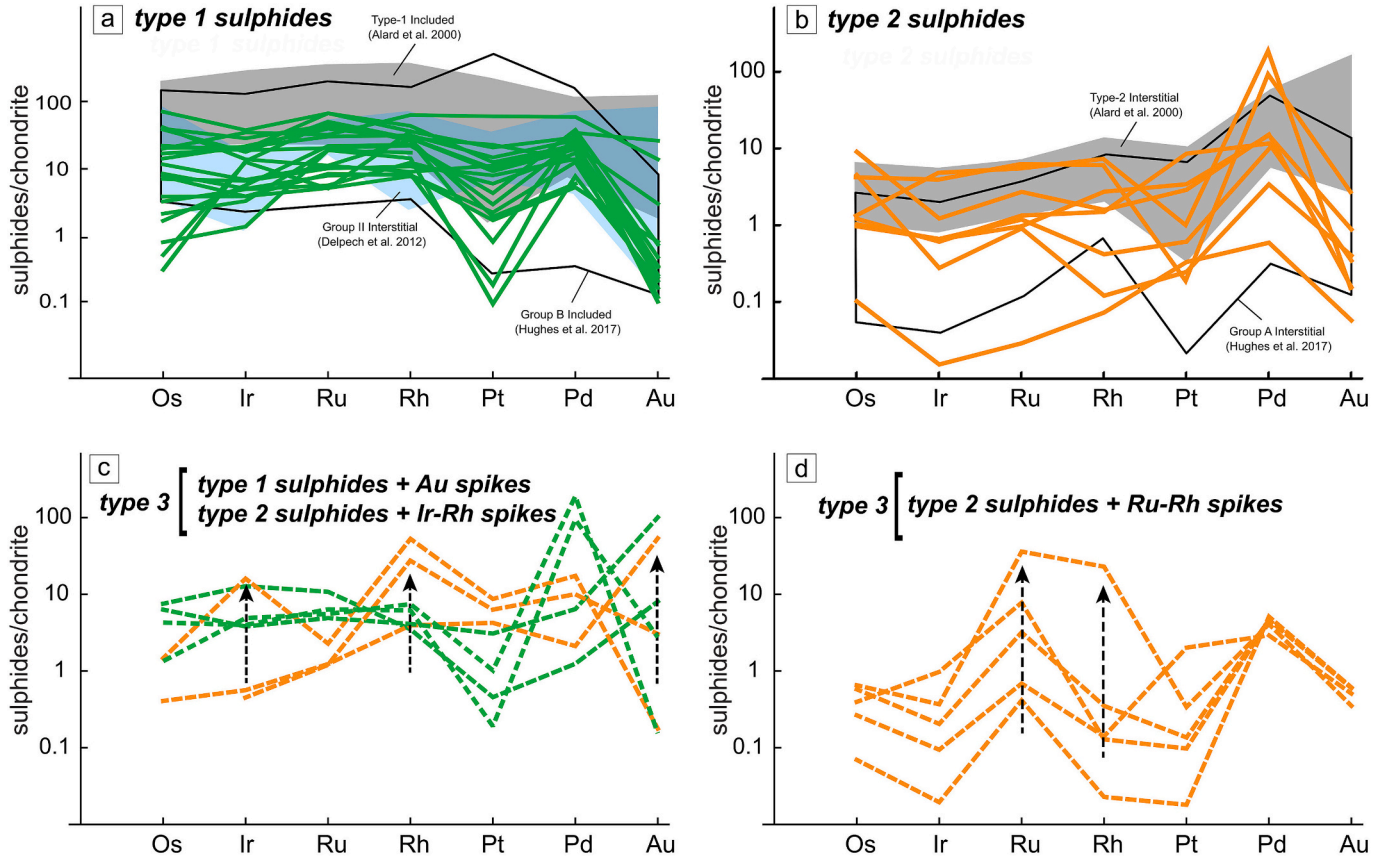

Fig. 13. Chondrite-normalized abundances of platinum-group elements (PGE) in base-metal sulphides (BMS) in Sant Corneli peridotite xenoliths. a) *Type-1* sulphide PGE patterns (green) compared to similar patterns in other studies: type-1 included sulphides (mantle peridotite xenoliths from alkali basalt) from Alard et al. (2000); Group II interstitial sulphides from Delpech et al. (2012); Group B included sulphides from Hughes et al., 2017. b) *Type-2* sulphide PGE patterns (orange) compared to similar patterns in other studies: type-2 interstitial sulphides (mantle peridotite xenoliths from alkali basalt) from Alard et al. (2000); Group A interstitial sulphides from Hughes et al. (2017). c-d) *Type-3* sulphide PGE patterns (green and orange dashed lines), with distinct spikes of Ir—Rh, Ru—Rh, and Au present in some of the patterns. (For interpretation of the references to colour in this figure legend, the reader is referred to the web version of this article.)

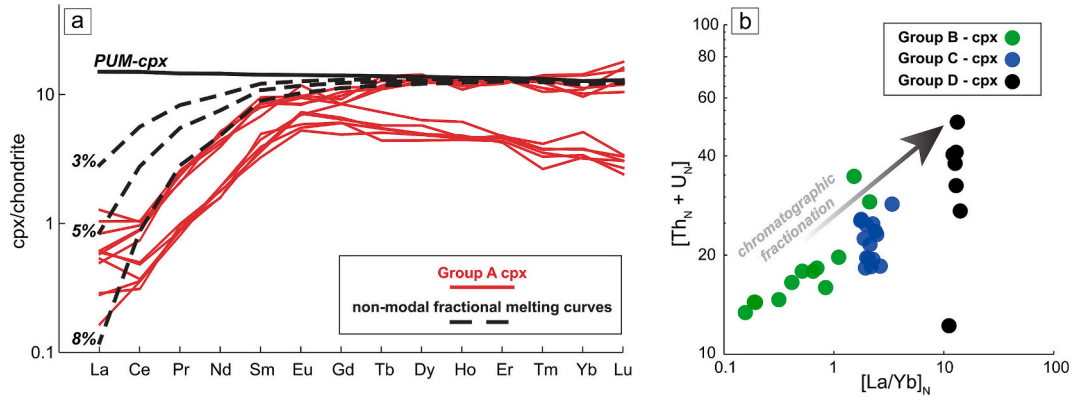

Fig. 14. a) Chondrite-normalized REE concentrations in clinopyroxene grains from Group A compared with non-modal fractional melting curves of clinopyroxene in PUM (black solid and dashed lines) in the spinel-peridotite facies (source and melting modal proportions olivine:orthopyroxene:clinopyroxene 0.54:0.28:0.18 and 0.11:0.59:0.53, respectively; Niu, 1997). Normalizing values from McDonough and Sun (1995). b) $[La/Yb]_N$ versus $[Th + U]_N$ for clinopyroxene grains from Groups B, C and D.

S tetrahedron (Fig. 16). In this scenario, a sulphide liquid may start crystallizing heazlewoodite-intermediate solid solution (*hzss-iss*) only as the temperature falls below ~900 °C (Craig and Kullerud, 1969; Helmy et al., 2021). Therefore, these phase relations indicate that the sulphides in Sant Corneli xenoliths were still completely molten at the high-temperature conditions (> 1100 °C) associated with the formation of the surrounding silicate glass within which they are entrained (Ballhaus et al., 2001; Craig and Kullerud, 1969; Helmy et al., 2021). In particular, the myrmekitic textural intergrowths frequently observed in Sant Corneli sulphides (Figs. 8–9) suggest a rapid quenching of the Ni-Cu-rich sulphide liquid while the mantle xenoliths were being brought to the surface (Ballhaus et al., 2001).

The PGE signatures of these glass-entrained sulphides may track whether their transport during melt percolation in the mantle occurred

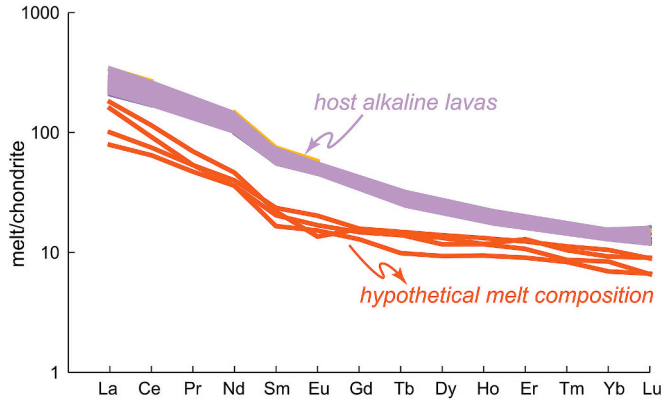

Fig. 15. Chondrite normalized REE concentrations reconstructed for the interstitial silicate melts compared with Quaternary host-alkaline basalts of La Garrotxa in the Catalan Volcanic Zone (Cebriá et al., 2000). Normalizing values from McDonough and Sun (1995).

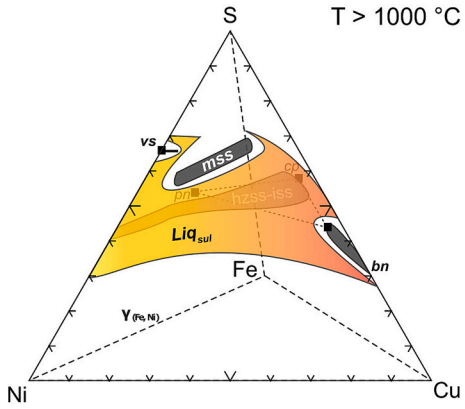

Fig. 16. Sulphide liquid field expected to occur in the S-Cu-Fe-Ni tetrahedron at 1000 °C. Mineral abbreviations: vs - vaesite; pn - pentlandite; cp - chalcopyrite; mss - monosulphide solid solution; hzss-iss - hazelwoodite solid solution-intermediate solid solution; bn – bornite.

as dissolved sulphur in sulphide-undersaturated silicate magmas (i.e., *chemical transport*, Mavrogenes and O'Neill, 1999), or as immiscible droplets of sulphide liquid in sulphide-saturated silicate magmas (i.e., *mechanical transport*; Ballhaus et al., 2006; Blanks et al., 2020; Schettino et al., 2023). In general, sulphide unmixing by immiscibility from the silicate magmas should not drive any significant inter-element fractionation between the PGEs (e.g. Type-1 included sulphides from Alard et al., 2000; Group II interstitial sulphides from Delpech et al., 2012; Group B included sulphides from Hughes et al., 2017), because of the very high sulphide/silicate melt partition coefficients of all these elements (Alard et al., 2011; Mann et al., 2012). Therefore, the nearly-flat chondrite-normalized PGE patterns of *type 1* sulphides (Fig. 13a), as well as their variable Pt negative anomalies, may be consistent with those expected for a parental sulphide liquid unmixing by sulphide-saturation in the silicate magmas, which could have released Pt-rich nanoparticles upon their interaction with the mantle peridotite (González-Jiménez et al., 2014, 2019; Schettino et al., 2024; Tassara et al., 2018). Although the *pn* ± *cp* mineral assemblage of *type 1* sulphide contrasts with the Fe-rich liquid composition expected to form by sulphide-immiscibility in mantle-derived magmas (Patten et al., 2013), Ni-Cu-rich sulphide droplets, like those documented in this study, have been reported to segregate under oxidizing magmatic conditions (Wohlgemuth-Ueberwasser et al., 2013). Progressive unmixing of sulphide liquid from the host-alkaline basalts at increasing fO_2 conditions may also account for the increasing Cu/Ni and S/Se ratios (Fig. 12d), and corresponding decreasing concentrations of PGE and TABS (Fig. 12f, h), of *type 1* sulphides (Alard et al., 2011; Delpech et al., 2012; Hughes et al., 2017). Similar PGE enrichment in metasomatic sulphides at increasing S/Se ratios may be also achieved by sulphidation reaction associated with the infiltration of CO_2-rich fluids (Delpech et al., 2012). However, the lack of any Os/Ir and Pd/Pt fractionation rules out this possibility (Alard et al., 2011; Hughes et al., 2017), corroborating the origin of these Ni-Cu-rich sulphide droplets by liquid immiscibility in silicate magmas attaining sulphide saturation at relatively oxidizing conditions (Delpech et al., 2012).

Conversely, the low IPGE abundances and supra-chondritic $[Pd/Ir]_N$ ratios in *type 2* sulphides (Fig. 13b), coupled with their Ni-Cu-rich major element compositions, are similar to those recorded in sulphide liquids originally extracted by incongruent melting of a residual Fe-rich *mss* in the mantle source (e.g. Type-2 Interstitial sulphides from Alard et al., 2000; Group A Interstitial sulphides from Hughes et al., 2017) (Alard et al., 2011; Ballhaus et al., 2006; Lorand and Luguet, 2016), and transported mechanically as immiscible droplets during magma ascent (Schettino et al., 2022, 2023). Indeed, such decreasing IPGE abundances in *type 2* sulphides cannot be accounted for noble metals fractionation upon fractional crystallization of sulphide liquid (Mansur et al., 2021), since no *hzss-iss* solid solution was expected to crystallize from the sulphide droplets at the high-temperature conditions (1110–1282 °C) recorded by their host glassy patches (Helmy et al., 2021). Whereas, the decreasing PGE contents in these sulphide droplets are associated with increasing Cu/Ni ratios (Fig. 12a), TABS concentrations (Fig. 12g-h) and extent of Pd_N/Ir_N fractionation (Fig. 12b), consistent with the trend expected by the extraction of Pd-, Cu- and chalcogenes-rich sulphide liquid by incongruent melting of residual *mss* in the mantle source of the host basalts (Ballhaus et al., 2006). Thus, the low IPGE contents and positively-sloped PGE patterns in *type 2* sulphides can be best explained by the retention of the IPGE in a residual *mss* undergoing incongruent melting in their mantle source, followed by the extraction of a Ni-Cu-rich sulphide liquid with supra-chondritic $[Pd/Ir]_N$ ratios (Ballhaus et al., 2006; Bockrath et al., 2004). In this scenario, the parental sulphide liquid of *type 2* sulphides was mechanically transported by ascending silicate magmas in form of immiscible droplets (Schettino et al., 2023), which held their PGE signatures inherited by sulphide liquid/*mss* chemical partitioning at the time of their physical extraction from the mantle source (Ballhaus et al., 2006; Bockrath et al., 2004).

Therefore, despite sharing a common major element composition, the different PGE signatures of *type 1* and *type 2* sulphides in Sant Corneli xenoliths underpin their derivation from two distinct generations of parental sulphide liquid: 1) a Ni-Cu-rich sulphide liquid segregated by sulphide-saturation by the host alkaline basalts during their interaction with the peridotite xenoliths (*type 1*), and; 2) a Ni-Cu-rich sulphide liquid originally extracted by incongruent melting from the mantle source and physically transported upwards by the host alkaline magmas in form of immiscible droplets (*type 2*).

5.4. *Nanoparticles incorporation/fractionation and implications for the precious metal budget of sulphide liquids*

The PGE compositions of *types 1* and *2* sulphides in Sant Corneli xenoliths are broadly consistent with those expected for a sulphide liquid equilibrating with a silicate melt or a residual *mss*, respectively. These two distinct PGE signatures are inherited by magma differentiation towards sulphide-saturated conditions during melt/rock reaction with mantle peridotite (*type 1* sulphides), or by partial melting at sulphide-saturated conditions in the mantle source (*type 2* sulphides). However, chemical equilibrium partitioning alone cannot explain the PGE signatures that are recorded by *type 3* sulphides (Fig. 13c-d). In general, *type 3* sulphides exhibit a range of major element compositions and $[Pd/Ir]_N$ fractionation broadly consistent with those of *types 1* and *2* sulphides (Fig. 12b), suggesting a common transport mechanism for their parental sulphide liquid during melt percolation in the mantle.

However, their original PGE signatures appear to be "disturbed" in some cases by the presence of pronounced positive anomalies in Ir—Rh, Au or Ru—Rh (Fig. 13c-d), which largely diverge from the patterns expected by sulphide liquid/silicate magmas or sulphide liquid/*mss* equilibrium partitioning (Ballhaus et al., 2006; Mungall and Brenan, 2014). These observations, together with the occurrence of precious metal-rich nanoparticles enclosed within the sulphides (Fig. 11a-d), support the hypothesis that the PGE signatures in the parental sulphide liquids of *type 3* sulphides were disturbed by the entrapment of pre-existing PGE-rich nanoparticles and/or nanomelts that were originally insoluble in the silicate magmas (González-Jiménez et al., 2019, 2021; Schettino et al., 2022, 2023). In fact, whether these nanoparticles were formed by exsolution at subsolidus temperatures would not have affected the PGE composition of the sulphides in which they were originally dissolved (Savelyev et al., 2018). Increasing number of experimental and empirical studies show that insoluble PGM nanoparticles and nanomelts may segregate in the silicate magmas (Anenburg and Mavrogenes, 2020; González-Jiménez et al., 2019, 2021) prior to the attainment of sulphide saturation (Maier et al., 2015; Wang and Li, 2023). These findings increasingly hint at the possibility that such immiscible PGE-rich nanoparticles and/or nanomelts may be preferentially transferred into the sulphide liquid by mechanical affinities (Schettino et al., 2023), exerting a key active role on the PGE enrichment of magmatic sulphide liquids (Liang et al., 2023).

The crystallization of early-magmatic PGE-rich nanoparticles from the silicate magmas may also produce an opposite effect involving PGE depletion, rather than enrichment, in the sulphide liquid (Liang et al., 2023; Park et al., 2013). This scenario may be properly applied for explaining the strong negative anomalies in Pt, relative to adjacent PGEs, that generally twist the otherwise nearly-flat PGE patterns of *type 1* sulphides (Fig. 13a). In fact, an early magmatic crystallization of Pt-rich sulphides (Coghill and Wilson, 1993; McDonald, 2008), arsenides (Maier et al., 2015) or alloys (Park et al., 2013) in the silicate magmas (Wang and Li, 2023), without their subsequent incorporation into the sulphide, would fractionate Pt from the other PGE during magmatic differentiation, yielding Pt-depleted sulphide liquids once sulphide-saturation is achieved (Liang et al., 2023).

All these observations indicate that, despite preserving a range of PGE distributions partially dictated by sulphide liquid/silicate magma and sulphide liquid/ *mss* equilibrium partitioning, the sulphides in Sant Corneli xenoliths have PGE abundances governed indeed by the mechanical incorporation, of early-magmatic segregation, of pre-existing PGE-rich nanoparticles and/or nanomelts. The formation of these insoluble PGE-rich nanoparticles in the silicate magmas may exert a key impact for enhancing the PGE budget of the sulphide liquid by mechanical entrapment, or yielding the opposite effect by selectively depleting in specific elements.

6. Conclusions

The study of sulphides within the spinel lherzolite xenoliths from the Sant Corneli volcano sheds light on the response of sulphides to melt percolation in the mantle and enhances our understanding of the geochemical and metallogenic features of the mantle beneath the northeastern Iberian Peninsula. Therefore, the main conclusions of this work can be summarized as follows:

1. Trace element composition of Sant Corneli clinopyroxene indicate that the SCLM beneath NE Iberia was extensively refertilized during an alkaline metasomatic event, which involved the progressive differentiation of alkaline silicate melts.
2. The sulphide-bearing interstitial silicate glass was formed through precipitation during a melt/rock reaction event triggered by the infiltration of the host alkaline basalts shortly before the rapid eruption of the host lava.
3. Clinopyroxene and spinel grains in contact with the interstitial glass exhibit coronitic rims formed through chemical interaction between the interstitial silicate melt and mantle peridotite, also right before the eruption.
4. The reported sulphides belong to the Ni-Cu-Fe-S compositional system and they are located within the interstitial silicate glass and the coronitic rims of clinopyroxene and spinel. The observed pentlandite ± bornite ± chalcopyrite assemblage, coupled with a general lack of pyrrhotite, indicates their origin from melts overlapping the compositional field of the central portion of the Fe-Ni-Cu-S system. The myrmekitic textural intergrowths frequently observed in Sant Corneli sulphides implies rapid quenching of the Ni-Cu-rich sulphide liquid during the ascent of mantle xenoliths to the surface.
5. Distinct PGE chondrite-normalized patterns in sulphides allow classification into three types. *Type 1* and *2* sulphides originated from two separate generations of parental sulphide melt. *Type 1* results from the segregation of Ni-Cu-rich sulphide liquid during sulphur saturation caused by the interaction of host alkaline basalts with peridotite xenoliths. On the other hand, *type 2* originates from a Ni-Cu-rich sulphide liquid initially extracted through incongruent melting from the mantle source and subsequently mechanically transported upward by host alkaline magmas in the form of immiscible droplets. *Type 3* sulphides are influenced by the entrapment of pre-existing PGE-rich nanoparticles and/or nanomelts that were originally insoluble in the silicate magmas. These nanoparticles play a crucial role in disturbing the distribution of PGE, resulting in pronounced positive anomalies in Ir—Rh, Au, or Ru—Rh. Therefore, the incorporation of early-magmatic PGE-rich nanoparticles during magmatic differentiation contributes to both PGE enrichment and depletion in the sulphide liquid.

Supplementary data to this article can be found online at https://doi.org/10.1016/j.lithos.2024.107820.

Author contributions

Conceptualization: MR, ES, MC, JMGJ; fieldwork and sampling: MR, MC, JMGJ, JAP, LP; methodology: MR, ES, MC, JMGJ, MG, RP, ML, OL, XL, validation of results: MR, ES, MC, JMGJ, RP; data curation: MR, ES, MC, JMGJ, MG, RP; writing-original draft preparation: MR, ES, MC, JMGJ; writing-review editing: MR, ES, MC, JMGJ, RP; supervision: MC, JMGJ; project administration: JMGJ, JAP; funding acquisition: MC, JMGJ, JAP. All authors revised the final version of the manuscript.

CRediT authorship contribution statement

Miguel Roquet: Writing – review & editing, Writing – original draft, Visualization, Validation, Methodology, Investigation, Formal analysis, Data curation, Conceptualization. **Erwin Schettino:** Writing – review & editing, Writing – original draft, Visualization, Validation, Formal analysis, Data curation, Conceptualization. **Marc Campeny:** Writing – review & editing, Writing – original draft, Validation, Supervision, Resources, Methodology, Investigation, Funding acquisition, Formal analysis, Data curation, Conceptualization. **José María González-Jiménez:** Writing – review & editing, Writing – original draft, Validation, Supervision, Resources, Project administration, Methodology, Investigation, Funding acquisition, Formal analysis, Data curation, Conceptualization. **Michel Grégoire:** Formal analysis, Data curation. **Rubén Piña:** Writing – review & editing, Writing – original draft, Validation, Formal analysis, Data curation. **Mathieu Leisen:** Formal analysis, Data curation. **Joaquín A. Proenza:** Resources, Project administration, Investigation, Funding acquisition. **Oscar Laurent:** Formal analysis, Data curation. **Llorenç Planagumà:** Investigation. **Xavier Llovet:** Formal analysis, Data curation.

Declaration of competing interest

The authors declare no competing interests. The funders had no role in the design of the study, in the collection of samples, the analyses, the interpretation of data, the writing of the manuscript nor the decision to publish these results.

Data availability statement

The authors confirm that the data supporting the findings of this study are available within the article and its supplementary materials.

Acknowledgements

This research has been made possible through the support of the Spanish Grant NANOMET PID2022-138768OB-I00 funded by MCIN/AEI/10.13039/50110001133 and by "ERDF A way of making Europe" by the "European Union". We are also grateful for the financial and logistical assistance provided by the Natural Sciences Museum of Barcelona (MCNB) and the Mineralogy Department of the Universidad de Granada. Special thanks are extended to Jesús Montes of the Universidad de Granada and Gerard Lucena for their meticulous efforts in the elaboration of polished thin sections. We express our gratitude to Alicia González of the Centro de Instrumentación Científica for her valuable assistance during HRSEM analyses. Additionally, we would like to acknowledge Joan Bastida of the Can Saboia quarries for granting access permission to the Sant Corneli outcrops, facilitating our sampling endeavours. Special thanks also to Jorgina Jordà, Màrius Asensi, Agustí Asensi and Josep Barnés for their support during the sampling.

References

Alard, O., Griffin, W., Lorand, J., Jackson, S., O'Reilly, S., 2000. Non-chondritic distribution of the highly siderophile elements in mantle sulphides. Nature 407, 891–894.
Alard, O., Lorand, J.P., Reisberg, L., Bodinier, J.L., Dautria, J.M., O'reilly, S.Y., 2011. Volatile-rich metasomatism in Montferrier xenoliths (Southern France): Implications for the abundances of chalcophile and highly siderophile elements in the subcontinental mantle. J. Petrol. 52, 2009–2045.
Anenburg, M., Mavrogenes, J.A., 2020. Noble metal nanonugget insolubility in geological sulphide liquids. Geology 48, 939–943.
Aulbach, S., Griffin, W.L., Pearson, N.J., O'Reilly, S.Y., Kivi, K., Doyle, B.J., 2004. Mantle formation and evolution, Slave Craton: constraints from HSE abundances and Re-Os isotope systematics of sulphide inclusions in mantle xenocrysts. Chem. Geol. 208, 61–88.
Ballhaus, C., Tredoux, M., Späth, A., 2001. Phase relations in the Fe–Ni–Cu–PGE–S system at magmatic temperature and application to massive sulphide ores of the Sudbury igneous complex. J. Petrol. 42, 1911–1926.
Ballhaus, C., Bockrath, C., Wohlgemuth-Ueberwasser, C., Laurenz, V., Berndt, J., 2006. Fractionation of the noble metals by physical processes. Contrib. Mineral. Petrol. 152, 667–684.
Barnes, S.J., Mungall, J.E., Le Vaillant, M., Godel, B., Lesher, C.M., Holwell, D., Lightfoot, P.C., Krivolutskaya, N., Wei, B., 2017. Sulphide-silicate textures in magmatic Ni-Cu-PGE sulphide ore deposits: Disseminated and net-textured ores. Am. Mineral. 3, 473–506.
Bertotto, G.W., Mazzucchelli, M., Giovanardi, T., Conceiçao, R.V., Zanetti, A., Schilling, M.E., Bernardi, M.I., Ponce, A.D., Jalowitzki, T., Gervasoni, F., Cipriani, A., 2022. Mantle Xenoliths from Huanul Volcano (Central-West Argentina): a Poorly Depleted Mantle Source under Southern Payenia. Geosciences 12 (4), 157.
Bianchini, G., Beccaluva, L., Bonadiman, C., Nowell, G., Pearson, G., Siena, F., Wilson, M., 2007. Evidence of diverse depletion and metasomatic events in harzburgite–lherzolite mantle xenoliths from the Iberian plate (Olot, NE Spain): Implications for lithosphere accretionary processes. Lithos 94 (1–4), 25–45.
Blanks, D.E., Holwell, D., Fiorentini, M., Moroni, M., Giuliani, A., Tassara, S., González-Jiménez, J.M., Boyce, A.J., Ferrari, E., 2020. Fluxing of mantle carbon as a physical agent for metallogenic fertilization of the crust. Nat. Commun. 11 (1), 4342.
Bockrath, C., Ballhaus, C., Holzheid, A., 2004. Fractionation of the platinum-group elements during mantle melting. Science 305, 1951–1953.
Bodinier, J., Vasseur, G., Vernieres, J., Dupuy, C., Fabries, J., 1990. Mechanisms of Mantle Metasomatism: Geochemical Evidence from the Lherz Orogenic Peridotite. J. Petrol. 31 (3), 597–628.
Borghini, A., Nicoli, G., Ferrero, S., O'Brien, P., Laurent, O., Remusat, L., Borghini, G., Milani, S., 2023. The role of continental subduction in mantle metasomatism and carbon recycling revealed by melt inclusions in UHP eclogites. Sci. Advanc. 9 (6).
Brenan, J., Bennett, N., Zajacz, Z., 2016. Experimental results on fractionation of the highly siderophile elements (HSE) at variable pressures and temperatures during planetary and magmatic differentiation. Rev. Mineral. Geochem. 81 (1), 1–87.
Cabri, L.J., 1973. New data on phase relations in the CuFe-S system. Econ. Geol. Bull. Soc. Econ. Geol. 68, 443–454.
Cebriá, J.M., López-Ruiz, J., Doblas, M., Oyarzun, R., Hertogen, J., Benito, R., 2000. Geochemistry of the Quaternary alkali basalts of Garrotxa (NE Volcanic Province, Spain): a case of double enrichment of the mantle lithosphere. J. Volcanol. Geotherm. Res. 102, 217–235.
Coghill, B.M., Wilson, A.H., 1993. Platinum-group minerals in the Selukwe Subchamber, Great Dyke, Zimbabwe: implications for PGE collection mechanisms and post-formational redistribution. Mineral. Mag. 1.
Craig, J.R., Kullerud, G., 1968. Phase relations and mineral assemblages in the copper-lead-sulfur system. Am. Mineral. 53, 145–161.
Craig, J.R., Kullerud, G., 1969. Phase Relations in the Cu-Fe-Ni-S System and Their Application to Magmatic Ore Deposits, in: Wilson, H.D.B. (Ed.), Magmatic Ore Deposits. Society of Economic Geologists (SEG), pp. 344–358.
Cruz, E., Galán, M., Fernández-Roig, M., Oliveras, V., Martínez, F.J., 2014. Types of Sulphides in Mantle Xenoliths from the Catalan Volcanic Zone (NE Spain). Macla 19.
Delpech, G., Lorand, J.P., Grégoire, M., Cottin, J.Y., O'Reilly, S.Y., 2012. In-situ geochemistry of sulphides in highly metasomatized mantle xenoliths from Kerguelen, southern Indian Ocean. Lithos 154, 296–314.
Dèzes, P., Schmid, S.M., Ziegler, P.A., 2004. Evolution of the European Cenozoic Rift System: interaction of the Alpine and Pyrenean orogens with their foreland lithosphere. Tectonophysics 389 (1–2), 1–33.
Fernández-Roig, M., Galán, G., 2015. Microestructuras y química mineral de lherzolitas en xenolitos mantélicos de Cataluña (NE España). Geogaceta 57, 3–6.
Fernández-Roig, M., Galán, G., Mariani, E., 2016. Crystal preferred orientation of olivine in mantle xenoliths from Catalonia (NE Spain). Trabajos de Geología (Universidad de Oviedo) 36, 119–138.
Galán, G., Oliveras, V., 2014. Melting and metasomatism in the lithospheric mantle of NE Spain: Geochemical and Sr-Nd isotopic characteristics. Chem. Geol. 366, 75–89.
Galán, G., Oliveras, V., Paterson, B., 2008. Types of metasomatism in mantle xenoliths enclosed in Neogene-Quaternary alkaline mafic lavas from Catalonia (NE Spain). Geol. Soc. Lond. Spec. Publ. 293, 121–153.
González-Jiménez, J.M., Villaseca-González, C., Griffin, W.L., O'Reilly, S.Y., Belousova, E., Ancochea, E., Pearson, N.J., 2014. Significance of ancient sulphide PGE and Re–Os signatures in the mantle beneath Calatrava, Central Spain. Contrib. Mineral. Petrol. 168, 1–24.
González-Jiménez, J., Roqué, J., Jiménez, A., Tassara, S., Nieto, F., Gervilla, F., Baurier, S., Proenza, J., Saunders, E., Deditius, A.P., Schilling, M., Corgne, A., 2019. Magmatic platinum nanoparticles in metasomatic silicate glasses and sulphides from Patagonian mantle xenoliths. Contrib. Mineral. Petrol. 174 (5), 47.
González-Jiménez, J.M., Tassara, S., Schettino, E., Roqué-Rosell, J., Farré-de-Pablo, J., Saunders, E., Deditius, A.P., Colás, V., Rovira-Medina, J.J., Dávalos, M.G., Schilling, M., Jiménez-Franco, A., Marchesi, C., Nieto, F., Proenza, J.A., Gervilla, F., 2020. Mineralogy of the HSE in the subcontinental lithospheric mantle - an interpretive review. Lithos 372–373.
González-Jiménez, J.M., Tretiakova, I., Fiorentini, M., Malkovets, V., Martin, L., Farré-de-Pablo, J., 2021. Nano- and Micrometer-Sized PGM in Ni-Cu-Fe Sulfides from an Olivine Megacryst in the Udachnaya Pipe, Yakutia, Russia. Can. Mineral. 59 (6), 1755–1773.
Griffin, W.L., Spetius, Z.V., Pearson, N.J., O'Reilly, S.Y., 2002. In situ Re-Os analysis of sulphide inclusions in kimberlitic olivine: new constraints on depletion events in the Siberian lithospheric mantle. Geochem. Geophys. Geosyst. 3, 11.
Hart, S.R., Dunn, T., 1993. Experimental Cpx/Melt Partitioning of 24 Trace elements. Contrib. Mineral. Petrol. 113, 1–8.
Hellebrand, E., Snow, J.E., Hoppe, P., Hofmann, A.W., 2002. Garnet-field Melting and Late-stage Refertilization in 'Residual' Abyssal Peridotites from the Central Indian Ridge. J. Petrol. 43 (12), 2305–2338.
Helmy, H.M., Botcharnikov, R., Ballhaus, C., Deutsch-Zemlitskaya, A., Wirth, R., Schreiber, A., Buhre, S., Häger, T., 2021. Evolution of magmatic sulphide liquids: how and when base metal sulphides crystallize? Contrib. Mineral. Petrol. 176, 1–15.
Hepworth, L., Stephen, J., Gertisser, R., Johnson, C., Emeleus, C., O'Driscoll, B., 2020. Rapid crystallization of precious-metal-mineralized layers in mafic magmatic systems. Nat. Geosci. 13, 375–381.
Holwell, D., Fiorentini, M., McDonald, I., Lu, Y., Giuliani, A., Smith, D.J., Keith, M., Locmelis, M., 2019. A metasomatized lithospheric mantle control on the metallogenic signature of post-subduction magmatism. Nat. Commun. 10, 3511.
Holwell, D., Fiorentini, M., Knott, T., McDonald, I., Blanks, D., McCuaig, T.C., Gorczyk, W., 2022. Mobilisation of deep crustal sulphide melts as a first order control on upper lithospheric metallogeny. Nat. Commun. 13 (1), 573.
Hughes, H.S., McDonald, I., Loocke, M., Butler, I.B., Upton, B.G., Faithfull, J.W., 2017. Paradoxical co-existing base metal sulphides in the mantle: the multi-event record preserved in Loch Roag peridotite xenoliths, North Atlantic Craton. Lithos 276, 103–121.
Ionov, D.A., Hofmann, A.W., Shimizu, N., 1994. Metasomatism-induced melting in mantle xenoliths from Mongolia. J. Petrol. 35, 753–785.
Ionov, D.A., Bodinier, J.L., Mukasa, S.B., Zanetti, A., 2002. Mechanisms and sources of mantle metasomatism: Major and trace element compositions of peridotite xenoliths from Spitsbergen in the context of numerical modelling. J. Petrol. 43, 2219–2259.
Jochum, K.P., Weis, U., Stoll, B., Kuzmin, D., Yang, Q., Raczek, I., Jacob, D.E., Stracke, A., Birbaum, K., Frick, D.A., Günther, D., Enzweiler, J., 2011. Determination of Reference Values for NIST SRM 610–617 Glasses following ISO guidelines. Geostand. Geoanal. Res. 35 (4), 397–429.

Johnson, K.T., Dick, H.J., Shimizu, N., 1990. Melting in the oceanic upper mantle: an ion microprobe study of diopsides in abyssal peridotites. J. Geophys. Res. Solid Earth 95, 2661–2678.
Liang, Q.L., Song, X.Y., Long, T.M., Wirth, R., Dai, Z.H., 2023. The effect of platinum-group minerals on differentiation of platinum-group elements in magmatic sulphide deposits: evidence from the Cu-Ni-PGE deposits in the Yangliuping area of the Emeishan large igneous province, SW China. Chem. Geol. 636, 121645.
Lorand, J.P., Alard, O., 2001. Platinum-group element abundances in the upper mantle: new constraints from in situ and whole-rock analyses of Massif Central xenoliths (France). Geochim. Cosmochim. Acta 65, 2789–2806.
Lorand, J.P., Luguet, A., 2016. Chalcophile and siderophile elements in mantle rocks: Trace elements controlled by trace minerals. Rev. Mineral. Geochem. 81, 441–488.
Lorand, J.P., Delpech, G., Grégoire, M., Moine, B., O'Reilly, S.Y., Cottin, J.Y., 2004. Platinum-group elements and the multistage metasomatic history of Kerguelen lithospheric mantle (South Indian Ocean). Chem. Geol. 208, 195–215.
Maier, W.D., Maattaa, S., Yang, S., Oberthur, T., Lahaye, Y., Huhma, H., Barnes, S.J., 2015. Composition of the ultramafic–mafic contact interval of the Great Dyke of Zimbabwe at Ngezi mine: Comparisons to the Bushveld complex and implications for the origin of the PGE reefs. Lithos 238, 207–222.
Mann, U., Frost, D., Rubie, D., Becker, H., Audetat, A., 2012. Partitioning of Ru, Rh, Pd, Re, Ir and Pt between liquid metal and silicate at high pressures and high temperatures. Implications for the origin of highly siderophile element concentrations in the Earth's mantle. Geochim. Cosmochim. Acta 84, 593–613.
Mansur, E., Barnes, S.J., Filho, C.F.F., 2021. The effects of post-cumulus alteration on the distribution of chalcophile elements in magmatic sulphide deposits and implications for the formation of low-S-high-PGE zones: the Luanga deposit, Carajás Mineral Province, Brazil. Can. Mineral. 59 (6), 1453–1484.
Martí, J., Mitjavila, J., Roca, E., Aparicio, A., 1992. Cenozoic magmatism of the Valencia trough (western Mediterranean): relationship between structural evolution and volcanism. Tectonophysics 203, 145–165.
Martí, J., Pujadas, A., Ferrés, D., Planagumà, Ll, Mallarach, J.M., 2001. El vulcanisme Guia de camp de la Zona Volcànica de la Garrotxa, first ed. Parc Natural de la zona volcánica de la Garrotxa, Olot.
Martí, J., Planagumà, L., Geyer, A., Canal, E., Pedrazzi, D., 2011. Complex interaction between Strombolian and phreatomagmatic eruptions in the Quaternary monogenetic volcanism of the Catalan Volcanic Zone (NE of Spain). J. Volcanol. Geotherm. Res. 201, 178–193.
Mavrogenes, J.A., O'Neill, H., 1999. The relative effects of pressure, temperature and oxygen fugacity on the solubility of sulphide in mafic magmas. Geochim. Cosmochim. Acta 63 (7–8), 1173–1180.
McDonald, I., 2008. Platinum-group element and sulphide mineralogy in ultramafic complexes at western Andriamena, Madagascar. Appl. Earth Sci. 117 (1), 1–10.
McDonough, W.F., Sun, S., 1995. The composition of the Earth. Chem. Geol. 120 (3–4), 223–253.
Miller, C., Zanetti, A., Thöni, M., Konzett, J., Klötzli, U., 2012. Mafic and silica-rich glasses in mantle xenoliths from Wau-en-Namus, Libya: textural and geochemical evidence for peridotite–melt reactions. Lithos 128 (131), 11–26.
Mungall, J.E., Brenan, J.M., 2014. Partitioning of platinum-group elements and au between sulphide liquid and basalt and the origins of mantle-crust fractionation of the chalcophile elements. Geochim. Cosmochim. Acta 125, 265–289.
Navon, O., Stolper, E., 1987. Geochemical consequences of melt percolation: the upper mantle as a chromatographic column. J. Geol. 95, 285–307.
Neumann, E.R., Wulff-Pedersen, E., 1997. The origin of highly silicic glass in mantle xenoliths from the Canary Islands. J. Petrol. 38, 1513–1539.
Nimis, P., Taylor, W., 2000. Single clinopyroxene thermobarometry for garnet peridotites. Part I. Calibration and testing of a Cr-in-Cpx barometer and an enstatite-in-Cpx thermometer. Contrib. Mineral. Petrol. 139, 541–554.
Niu, Y., 1997. Mantle Melting and Melt Extraction Processes beneath Ocean Ridges: evidence from Abyssal Peridotites. J. Petrol. 38 (8), 1047–1074.
Norman, M., 1998. Melting and metasomatism in the continental lithosphere: Laser ablation ICPMS analysis of minerals in spinel lherzolites from eastern Australia. Contrib. Mineral. Petrol. 130 (3), 240–255.
Oliveira, B., Alfonso, J., Tilhac, R., 2020. A Disequilibrium Reactive Transport Model for Mantle Magmatism. J. Petrol. 61.
Pan, S., Zheng, J., Yin, Z., Griffin, W.L., Xia, M., Lin, A., Zhang, H., 2018. Spongy texture in mantle clinopyroxene records decompression-induced melting. Lithos 320, 144–154.
Park, J.W., Campbell, I.H., Arculus, R.J., 2013. Platinum-alloy and Sulphur saturation in an arc-related basalt to rhyolite suite: evidence from the Pual Ridge lavas, the Eastern Manus Basin. Geochim. Cosmochim. Acta 101, 76–95.
Paton, C., Hellstrom, J., Paul, B., Woodhead, J., Hergt, J., 2011. Iolite: Freeware for the visualization and processing of mass spectrometric data. J. Anal. At. Spectrom. 26, 2508.
Patten, C., Barnes, S.J., Mathez, E.A., Jenner, F.E., 2013. Partition coefficients of chalcophile elements between sulphide and silicate melts and the early crystallization history of sulphide liquid: LA-ICP-MS analysis of MORB sulphide droplets. Chem. Geol. 358, 170–188.
Putirka, K., 2008. Thermometers and Barometers for Volcanic Systems, Minerals, Inclusions and Volcanic Processes, Reviews in Mineralogy and Geochemistry. Mineralogic. Soc. Am. 69, 61–120.
Rampone, E., Borghini, G., Basch, V., 2020. Melt migration and melt-rock reaction in the Alpine-Apennine peridotites: Insights on mantle dynamics in extending lithosphere. Geosci. Front. 11, 151–166.
Revelles, J., Martí-Molist, J., Burjachs, F., Finsinger, W., Iriarte, E., Mesquita-Joanes, F., Pla-Rabés, S., Planagumà, L., Rodrigo, M.A., Alcalde, G., Saña, M., 2023. Socio-ecological impact of monogenetic volcanism in the La Garrotxa Volcanic Field (NE Iberia). Sci. Rep. 13 (1), 8168.
Rielli, A., Tomkins, A.G., Nebel, O., Brugger, J., Etschmann, B., Evans, K.A., Wykes, J.L., Vasilyev, P., Paterson, D.J., 2022. Incipient metal and sulfur extraction during melting of metasomatised mantle. Earth Planet. Sci. Lett. 599.
Roca, E., 2001. The Northwest Mediterranean Basin (Valencia Trough, Gulf of Lions and Liguro Provencal basins): Structure and geodynamic evolution. Mémoires du Muséum National d'Historie Naturelle 186, 671–706.
Savelyev, D.P., Kamenetsky, V.S., Danyushevsky, L.V., Botcharnikov, R.E., Kamenetsky, M.B., Park, J., Portnyagin, M.V., Olin, P., Krasheninnikov, S.P., Hauff, F., Zelenski, M.E., 2018. Immiscible sulphide melts in primitive oceanic magmas: evidence and implications from picrite lavas (Eastern Kamchatka, Russia). Am. Mineral. 103, 886–869.
Schettino, E., Marchesi, C., González-Jiménez, J., Saunders, E., Hidas, K., Gervilla, F., Garrido, C.J., 2022. Metallogenic fingerprint of a metasomatized lithospheric mantle feeding gold endowment in the western Mediterranean basin. Geol. Soc. Am. 134 (5–6), 1468–1484.
Schettino, E., González-Jiménez, J.M., Marchesi, C., Palozza, F., Blanco-Quintero, I., Gervilla, F., Braga, R., Garrido, C., Fiorentini, M., 2023. Mantle-to-crust metal transfer by nanomelts. Nat. Commun. 4, 256.
Schettino, E., González-Jiménez, J.M., Marchesi, C., Dávalos-Elizondo, M.G., Camprubí, A., Colás, V., Saunders, E., Aranda-Gómez, J.J., Griffin, W.L., 2024. A fragment of inherited Archaean lithospheric mantle rules the metallogeny of Central Mexico. Int. Geol. Rev. 66 (1), 6–30.
Sedano, José, 2019. Gravimetria del sector NO de la fossa del Vallès (Granollers – La Garriga). Universitat Politècnica de Catalunya, Escola de Camins.
Shaw, C., Heidelbach, F., Dingwell, D., 2006. The origin of reaction textures in mantle peridotite xenoliths from Sal Island, Cape Verde: the case for "metasomatism" by the host lava. Contrib. Mineral. Petrol. 151, 681–697.
Tassara, S., González-Jiménez, J.M., Reich, M., Morata, D., Barra, F., Grégoire, M., Saunders, J.E., Cannatelli, C., 2017. Refertilization of the Subcontinental Lithospheric Mantle and its Link to the Formation of Metallogenic Provinces. American Geophysical Union, p. 53.
Tassara, S., González-Jiménez, J.M., Reich, M., Saunders, E., Luguet, A., Morata, D., Grégoire, M., Acken, D., Schilling, M.E., Barra, F., Nowell, G., Corgne, A., 2018. Highly siderophile elements mobility in the subcontinental lithospheric mantle beneath southern Patagonia. Lithos 314-315, 579–596.
Tassara, S., Reich, M., Konecke, B.A., González-Jiménez, J.M., Simon, A.C., Morata, D., Barra, F., Fiege, A., Schilling, M.E., Corgne, A., 2020. Unravelling the Effects of Melt–Mantle Interactions on the Gold Fertility of Magmas. Front. Earth Sci., 8, 29.
Wang, W., Li, Y., 2023. Platinum solubility in silicate melts: the effects of sulfur (S^{2-}), temperature, and melt composition. Geochim. Cosmochim. Acta 361, 113–132.
Wilson, M., Downes, H., 1992. Mafic alkaline magmatism associated with the European Cenozoic Rift System. Tectonophysics, 208, 1–3, 173–182.
Wohlgemuth-Ueberwasser, C.C., Fonseca, R.O.C., Ballhaus, C., Berndt, J., 2013. Sulphide oxidation as a process for the formation of copper-rich magmatic sulphides. Mineral. Deposita 48, 115–127.